

Optical and radio properties of extragalactic radio sources with recurrent jet activity

A. Kuźmicz,^{1,2,3*} M. Jamrozy,² D. Kozieł-Wierzbowska² and M. Weżgowiec²

¹Center for Theoretical Physics, Polish Academy of Sciences, Al. Lotników 32/46, 02-668 Warsaw, Poland

²Astronomical Observatory, Jagiellonian University, ul. Orła 171, 30-244 Krakow, Poland

³Queen Jadwiga Astronomical Observatory in Rzepiennik Biskupi, 33-163 Rzepiennik Strzyżewski, Poland

Accepted XXX. Received YYY; in original form ZZZ

ABSTRACT

We present a sample of 74 radio sources with recurrent jet activity. The sample consists of 67 galaxies, 2 quasars, and 5 unidentified sources, selected from the published data as well as newly recognized. The sample’s redshift range is $0.002 < z < 0.7$ and the size of inner and outer structures varies from 0.02 to 4248 kpc. We analyse the optical and radio properties of the sample and compare them with the characteristics of ordinary one-off FRII radio sources. With the help of stellar population modelling we derive black hole masses and stellar masses of host galaxies of 35 restarting radio sources, finding that the black hole masses in restarting radio sources are comparable to those of typical single cycle FRII radio sources. The obtained median values of $\log M_{\text{BH}}$ are 8.58 M_{\odot} and 8.62 M_{\odot} , respectively. Unlike the black hole masses, the stellar masses in restarting radio sources tend to be smaller than in the FRII sources. Although the stellar populations of the hosts of recurrent activity sources are dominated by old stars, a significant fraction of young stars can be observed as well. Based on the SDSS photometric observations, we also analyse the morphology of the host galaxies and obtained significantly smaller concentration indices for the restarting radio sources when compared to the classical FRII hosts. This effect can be interpreted as a result of frequent merger events in the history of host galaxies of restarting radio sources.

Key words: galaxies: active – galaxies: nuclei – galaxies: structure – galaxies: jets – radio continuum: galaxies.

1 INTRODUCTION

The classic extragalactic radio sources have been investigated for much over a half of century; for instance, Baade & Minkowski (1954) found an optical counterpart for the Cygnus A source as long ago as 1954). The most widely assumed underlying model of radio sources comprises a fast rotating supermassive black hole (SMBH) accompanied by an accretion disk. The transfer of disk energy to the external lobes is accomplished through powerful relativistic jets (Scheuer 1974). The jet activity phases are rather brief ($\sim 10^8$ yrs) in comparison with the entire life time of the host galaxy ($\sim 10^{10}$ yrs). However, the activity of a jet can restart after a period of silence. This phenomenon depends strictly on the physical conditions in the vicinity of the central SMBH. The presence of sources of peculiar character, classified neither as FRI nor FRII (Fanaroff & Riley 1974), could indicate a recurring AGN activity. The active galactic nuclei

in general can be classified into a number of separate categories; among others, the radio galaxies with two or more pairs of lobes extending from the core along the same axis, called double-double radio sources (DDRS; Schoenmakers et al. 2000). This group is rather sparse, with just about 45 objects recognized to date (for a review and references, see Saikia & Jamrozy 2009; Nandi & Saikia 2012). There are DDRSs of much different sizes, from merely scores of parsecs up to over one megaparsec. Besides the axial symmetric sources there is another type of recurrent activity radio galaxies. These are objects exhibiting large-scale diffuse relic radio emission that is due to an earlier cycle of activity. Such relics can be seen around compact powerful young radio sources (e.g. Baum et al. 1990). A separate group are so-called ‘X-shaped’ radio sources, which are also regarded as recurrent radio sources (e.g. Merritt & Ekers 2002; Sarpalli & Subrahmanyan 2009). We are not going to analyse these sources here, as their optical properties were studied already by Mezcuca et al. (2011, 2012).

* E-mail: cygnus@oa.uj.edu.pl

The fact that in some radio galaxies two or even three

pairs of lobes can be observed implies that the time required for the jet flow to cease is shorter than that for the outer lobes to fade. Thus, as the energy transported by the jets is able to last through the quiescent phase within their extended lobes, the radio galaxies can hold memory of the previous AGN activity. [Konar et al. \(2013\)](#) determined the duration of the inactive period for some DDRSs to be of the order of several million years. Interestingly enough, this time is too long to be explained in the frame of the currently existing theoretical models that describe properties of an AGN (e.g. accretion disk instability with the idle time of about 10^4 years; [Czerny et al. 2009](#)). On the other hand, it is too short for a new disk to form. Therefore, alternative theories have been formulated. The interruptions in the jet production mechanism could have been possibly caused by refuelling of the central engine. [Liu et al. \(Liu 2004; Liu et al. 2003, 2012\)](#) suggested that this kind of objects may arise due to interactions of SMBH binaries with the accretion disk. In such a picture, the secondary black hole (BH) drifts towards the centre, disrupting the inner parts of the accretion disk. After the both black holes merge, the gap widens, effectively stopping the process of jet formation. Such a behaviour could be expected in the case of the blazar OJ287 ([Valtonen et al. 2008](#)), which possesses two SMBHs, the smaller of which orbits the larger companion, surrounded by an accretion disk, with a period of about 11 years. The jet activity may start again at a later time, triggered by new matter flowing into the inner region. Consequently, a DDRS is created. The accepted belief that the multiple pair of lobes are produced by recurrent jet activity was questioned by [Wagner & Bicknell \(2011\)](#), who noted that such objects could also be produced by random emergence of radio plasma from an inhomogeneous, porous ISM. However, in this scenario we cannot expect an ideally symmetric interstellar medium (ISM) on both sides of the central AGN. This in turn would make it difficult to explain the existence of DDRSs with linearly symmetric inner lobes.

The AGNs with repeated jet activity could affect both the parent galaxy and the diffuse extended radio structure. Therefore, some properties of the objects with multiple activity cycles can be different from the radio galaxies with single activity.

[Wagner & Bicknell \(2011\)](#) found that there is a considerable transfer of energy and momentum to the ISM, and that the jets with powers of $10^{43} - 10^{46}$ erg s⁻¹ can inhibit star formation in the galactic core. This would influence the evolution of the galaxy. Therefore, the repeated jet activity could have implications for feedback processes of the parent galaxy.

[Subrahmanyan et al. \(1996\)](#) postulated that recurrent activity influences the linear size of radio sources. Therefore, at least some of the giant radio galaxies could become quite large because their central AGNs experienced several jet activity cycles. The jets of restarted cycles move not in the original intergalactic medium (IGM) but in a less dense environment of the primordial lobes, which allows them to reach further distances in a shorter time. Nevertheless, the mechanism underlying formation of the inner lobes is not yet fully understood. There are two plausible models suggested in the literature that could explain this. In the first model, called the ‘classical FRII model’, the inner lobes are formed in the same way as the lobes of typical ‘single-cycle’ radio galax-

ies. The inner lobes propagate through a denser medium than could be expected from purely synchrotron-emitting plasma, because thermally emitting material is drawn into the outer lobes of DDRSs during their growth and quiescent phases ([Kaiser 2000](#)). The second model, called the ‘bow-shock model’, assumes that the inner lobes are created by reaccelerating of the outer cocoon particles at the bow-shock created by almost ballistically moving jet heads ([Brocksopp et al. 2007, 2011; Safouris et al. 2008](#)). Both the ‘classical FRII’ and the ‘bow-shock’ models may need to be employed simultaneously to fully describe the dynamics and the structure of inner lobes.

Surprisingly enough, only recently it was realised that the jet activity can be a multiple phenomenon. The main reason for this is that such objects are not too frequent among radio galaxies. Furthermore, it is not too easy to recognize a restarting radio source, since the radio structures usually come from separate activity cycles and have significantly different surface brightnesses, angular extents, and spectral profiles. The ideal instance of a DDRS would be an object with bright detached pairs of lobes but most often the structures produced by consecutive cycles merge together. [Parma et al. \(1999\)](#) selected a class of radio galaxies, which possess spectra that steepen outwards, from the core to the outer edge of lobes. Most of them are narrow-angle-tail (NAT) or wide-angle-tail (WAT) radio galaxies, while within these two types of objects we can still find sources with multiple jet activity. In order to distinguish them and understand the cycles and the phases of interruption of the jet flow, it is crucial to determine ages of charged particles in different regions within the radio lobes. In order to fully recognize the recurrent activity phenomenon a statistical study of an extended sample is essential.

In this paper, we present the first systematic study of extragalactic radio sources with structures showing recurrent jet activity. We analyse the optical and radio properties of a large sample of restarting radio sources and compare them with characteristics of ordinary FRII radio galaxies, in order to learn more about the causes underlying episodic jet activity. In the next section, we briefly describe the source samples used for the analysis. The observations, data reduction, and processing are described in the third section, while in the fourth section we review and discuss the results. The conclusions are presented at the end of the paper. Throughout the paper, a flat vacuum-dominated universe with $\Omega_m=0.27$, $\Omega_\Lambda=0.73$ and $H_0=71$ km s⁻¹ Mpc⁻¹ is assumed.

2 THE SAMPLE

The recent studies by [Saikia & Jamrozy \(2009\)](#) and [Nandi & Saikia \(2012\)](#) significantly extend the number of sources which show multiple jet activity. It was noticed that multi-cycle jet activity is not just specific to giant objects, but is manifested also by smaller radio galaxies (with outer structures having sizes of only several hundred kiloparsecs). Nevertheless, such objects are not too well studied and still a number of physical parameters, e.g. the duration of an inactive phase, need better estimates.

Our sample of restarting radio sources contains 74 objects, including 67 galaxies, 2 quasars, and 5 uniden-

tified sources. The selection was based mostly on the published data, but we also included new sources, recognized recently by the authors of this paper. The redshifts for our sample objects range from 0.002 to 0.7. The only exception is J2107+2331, whose redshift is as high as $z=2.48$. The radio structures show a wide range of projected linear sizes – from 0.02 to 876 kpc for the inner to 48 to 4248 kpc for the outer lobes. In our sample there are 8 newly recognized restarting radio sources: J0042-0613, J0504+3806, J0914+1006, J0924+0602, J1004+5434, J1021+1216, J1520-0546, J1528+0544. All of them were identified using maps from the 1.4 GHz Faint Images of the Radio Sky at Twenty centimeters (FIRST; Becker et al. 1995) survey and the NRAO VLA Sky Survey (NVSS; Condon et al. 1998). The redshifts of these objects are within the range from $z=0.04$ to $z=0.31$. A half of the newly recognized restarting radio sources are giants with projected linear sizes larger than 0.7 Mpc (taking into account the sizes of the outer radio lobes). In most of the newly discovered sources the inner radio lobes have medium linear sizes, but there is one source J1528+0544 with a very compact (of 15 kpc) inner structure as well as one source J1021+1216 with very extended (876 kpc) inner doubles. In our sample, we consider also two X-shaped radio galaxies, i.e. J0009+1244 and J1513+2607. While we do not analyse this type of sources in this paper in general, these two sources are of peculiar type. Besides the usual X-shape morphology, they possess an additional pair of lobes in their central region. The sample presented in this paper is not complete, yet it is quite representative of the class. It covers a wide range of physical parameters, thus it is sufficiently large and diverse to allow for performing an analysis of their fundamental properties. There are a lot of candidates in the literature for a restarting radio source with structures that still have to be confirmed as multi-episodic (e.g. Nandi & Saikia 2012). Most of them either do not have optical identifications, or the resolution of the available radio maps is not sufficient to properly reveal their structure. We also expect a number of new multi-cycle source detections in the next few years from deep survey observations with new low-frequency radio telescopes (e.g. the Low Frequency Array; van Haarlem et al. 2013, the Long Wavelength Array; Ellingson et al. 2009, and the Murchison Widefield Array; Lonsdale et al. 2009).

We divided the radio sources from our sample according to their radio morphology into two classes: typical double-double radio sources, where two pairs of radio lobes are clearly visible (class A) and radio sources with prominent inner structure, surrounded by diffuse outer structures (class B). We classified 63 radio sources studied in this paper as class A objects, while only 11 belong to the class B.

The restarting radio sources and their basic properties are listed in Table 1, where the newly recognized radio sources are denoted with boldface. The radio maps are presented in Appendix A – class A radio sources and Appendix B – class B.

As a comparison sample, we used the FRII-type radio galaxies from Koziel-Wierzbowska & Stasińska (2011), where the optical and radio data were provided. This sample contains 401 FRII radio galaxies with a wide range of radio powers and sizes of radio structures. Ten of the FRII radio galaxies from the comparison sample show a double-double radio structure, and therefore were not used. Instead,

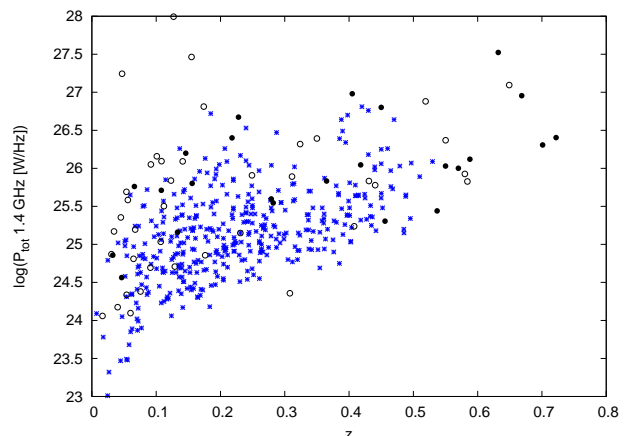


Figure 1. Sample of recurrent jet activity radio sources (black open and filled circles) and the comparison sample (blue asterisks) on the 1.4 GHz total radio luminosity–redshift plane. The recurrent radio sources with available spectra are marked as open black circles.

they were included in the sample of restarting sources. As a result, the final comparison sample consists of 391 sources.

Radio sources from both the samples are presented in Figure 1, where the relation between the distribution of the 1.4 GHz total radio luminosity and the redshift is plotted. The source with exceptionally high redshift (J2107+2331) is not shown in this figure.

3 OBSERVATIONAL DATA

In our analysis of recurrent jet activity sources we use both optical and radio data.

3.1 Optical evidence

The optical data are taken mainly from the SDSS Data Release 10 (DR10; Ahn et al. 2014). The photometric data were available for 53 radio sources and the spectroscopic data were available for 30 objects.

Spectroscopic data of further four objects (J0301+3512, J1651+0459, J1844+4533, J2048+0701) were taken from the archives of the Telescopio Nazionale Galileo (TNG) and the 5-meter Hale telescope at the Palomar Observatory. The observations and reduction procedures are described in Ho, Filippenko & Sargent (1995) and Buttiglione et al. (2009).

Additional spectra for six objects were obtained with our dedicated spectroscopic observations using the South African Astronomical Observatory (SAAO) telescopes and the William Herschel Telescope (WHT). Details of the WHT observations and data reduction are presented below. Spectra of J1520-0546 and J1528+0544 were obtained with the 1.9-m SAAO telescope equipped with the Cassegrain Grating Spectrograph. The optical spectra and description of observations are provided in Machalski et al. (2007).

WHT spectra: Spectral observations of four DDRGs, J0042-0613, J1835+6204, J2223-0206, and J2345-0449 were carried out with the WHT at the Roque de los Muchachos Observatory in La Palma, Spain. The observations were

obtained in the service mode on July 29th, 2009. The long-slit spectra were taken using the Intermediate Dispersion Spectrograph and Imaging System Double-Armed Spectrograph, which permit simultaneous observations in both blue and red filters. The slit of a width of $2''$ was centred on the nuclei of the sources and positioned along the jet axis of the radio galaxy. The integration time was split into several exposures to reduce the influence of cosmic rays. Spectra of two spectrophotometric standards, i.e. SP2011+065 and SP0031-124 were obtained for a proper intensity calibration. Arc lamp spectra were taken before and/or after target observations to allow for an accurate wavelength calibration. The average seeing during the observing run was about $1.2''$. The WHT spectra of these restarting radio galaxies have not been published to date and we present them in Figure 2.

The WHT data were reduced using the IRAF NOAO packages¹. Reduction steps were performed separately for each spectral range. The master bias frame was created by averaging all the bias frames obtained during the observing night and subtracted from the science frames. The master flat field frame was also created and all 2D-science frames were corrected for flat field. Then, the cosmic rays were removed from the science exposures. Wavelength calibration was performed using ArNe lamp exposures and verified by using sky lines. Next, a correction for optical distortion was applied. The contribution from the sky was determined from the sky regions at both sides of the resulting spectrum and subtracted. The 1D-spectra extraction was performed using the APALL task. The scientific exposures were flux-calibrated using exposures of the suitable spectrophotometric standard stars. In order to obtain the resulting spectra with a better S/N ratio, all the calibrated one-dimensional spectra of a given galaxy were combined.

The spectroscopic data of good quality are available only for 37 galaxies of the 74 restarting radio sources. Despite that, the galaxies with spectroscopic data are representative for the whole sample. In Figure 1 we marked the galaxies with available optical spectra. It can be seen that the distribution of galaxies with spectra is uniform and spans a wide range of redshifts and total radio luminosities. In Figure 3 we plotted the distributions of SDSS *r* magnitudes for both the samples. The sample of FR II radio galaxies contains only objects with optical spectra and is limited to *r* band magnitudes brighter than 22. The distribution for restarting radio galaxies is more uniform and optical spectra are available for the brighter objects in sample, but the range of magnitudes for the galaxies with spectra is similar as for the comparison sample.

3.2 Radio maps

In our radio analysis we measured the angular sizes and flux densities of inner and outer radio lobes using mainly maps from the 1.4 GHz FIRST and the NVSS radio surveys. For a few sources for which no data were available in NVSS/FIRST, or for which it was not possible to obtain precise measurements of angular sizes and flux densities using NVSS/FIRST, we took the relevant parameters from

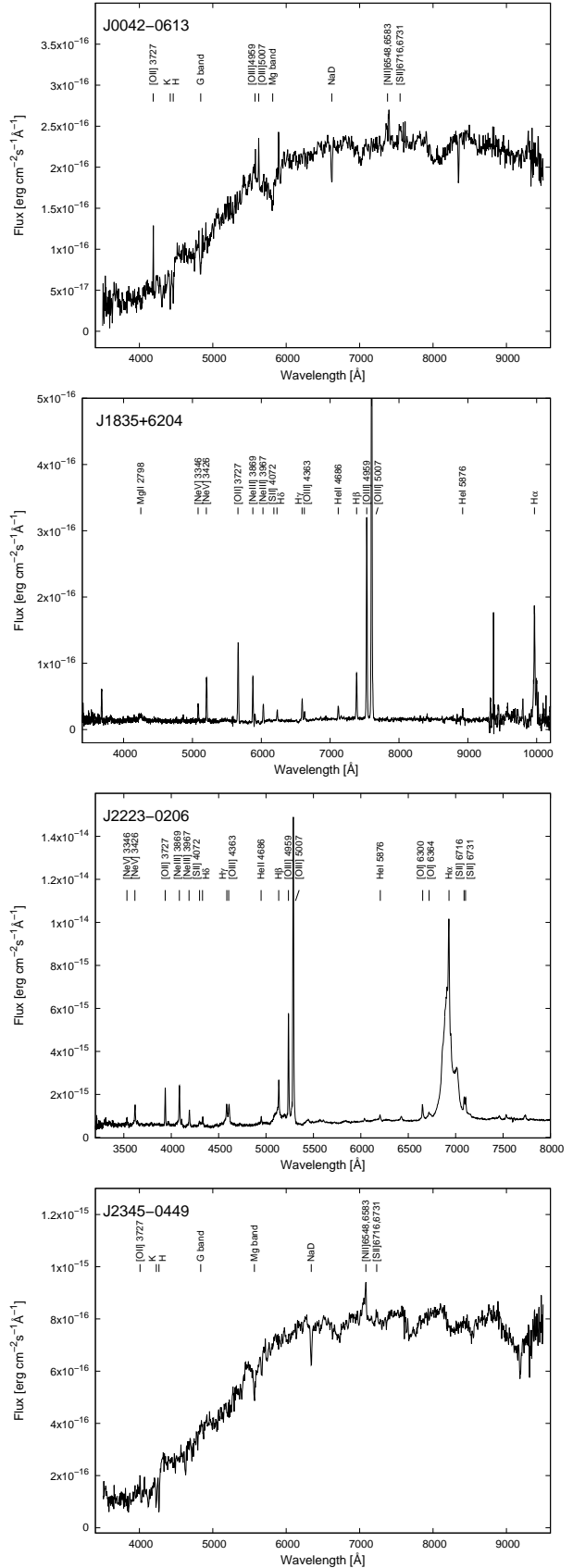


Figure 2. The optical WHT spectra of J0042–0613, J1835+6204, J2223–0206, and J2345–0449 restarting radio galaxies.

¹ <http://iraf.noao.edu>

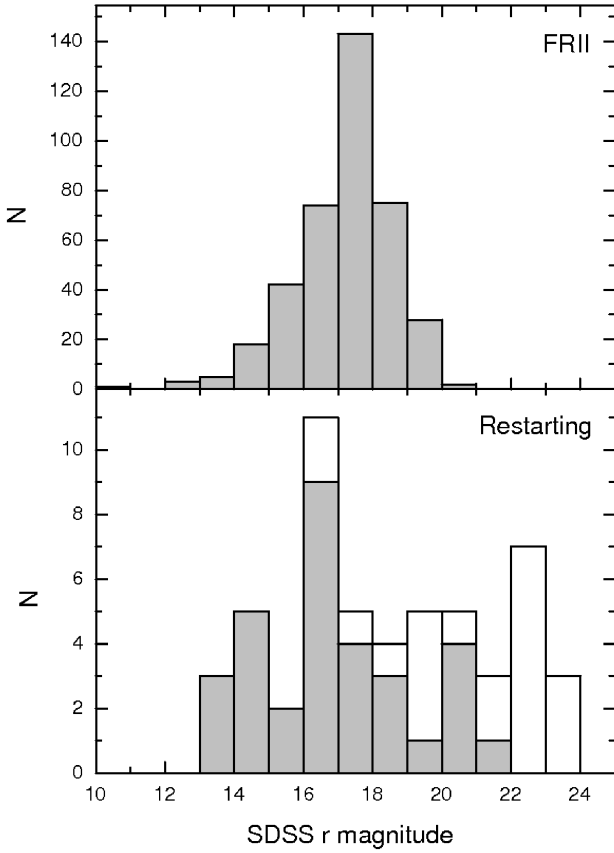


Figure 3. SDSS r magnitude distribution for FRII radio galaxies (**top**) and restarting radio galaxies (**bottom**). The radio galaxies with available optical spectra are plotted as a solid grey boxes, both for the restarting sample and the comparison one.

the literature given in Table 1.

3.3 Data analysis

The optical spectra of restarting radio sources have been used to measure the basic properties of the hosts of AGNs. We applied the stellar population synthesis code STARLIGHT² (Cid Fernandes et al. 2005) to model the observed spectrum. Stellar continuum was fitted basing on the superposition of 150 stellar spectra templates (extracted from the evolutionary synthesis models of Bruzual & Charlot 2003) with various ages and metallicities. Apart from continuum fitting, the STARLIGHT modelling gives the information about such parameters like star formation, chemical enrichment, and velocity dispersion.

To determine BH masses, we used the $M_{BH} - \sigma_*$ method. It is based on a tight correlation between the BH mass and the velocity dispersion of the stars in the galactic bulge (σ_* ; Ferrarese & Merritt 2000, Gebhardt et al. 2000), which is

described by the relation

$$\log\left(\frac{M_{BH}}{M_{\odot}}\right) = \alpha + \beta \log\left(\frac{\sigma_*}{200 \text{ km s}^{-1}}\right) \quad (1)$$

where the constants are $\alpha = 8.13 \pm 0.05$ and $\beta = 5.13 \pm 0.34$ (Graham et al. 2011).

For the two quasars (J0741+3112 and J0935+0204) we used their BH mass estimates based on the H_{β} mass scaling relation given by Shen et al. (2008).

The radio luminosity of the inner (P_{in}) and outer (P_{out}) radio lobes was calculated using the following formula given by Brown, Webster & Boyle (2001)

$$\log P(WHz^{-1}) = \log S(mJy) - (1 + \alpha) \cdot \log(1 + z) + 2 \log(D_L(Mpc)) + 17.08 \quad (2)$$

where α is the spectral index³ and D_L is a luminosity distance. The flux densities of the inner (S_{in}) and outer lobes (S_{out}) of individual sources were measured in the available maps and then listed in Table 1. Following e.g. Kellermann & Owen (1988), we adopted a typical spectral index value of $\alpha = -0.75$ for the inner and $\alpha = -1$ for the outer radio structures.

4 RESULTS

In this section, we compare some of the basic characteristics (radio morphology, physical parameters of host galaxy) of restarting radio galaxies with those of typical radio sources using the optical, radio and infrared data described above.

4.1 Optical properties

Using the Starlight Synthesis Code, we modelled the stellar continuum in spectra of 35 galaxies from our sample (except for two quasars) for which spectroscopic data were available. We obtained the information about a mixture of stellar populations present in a individual galaxies. It can be expressed by the light-fraction population vector x_j , which gives the percentage fraction of a galaxy light (luminosity) that comes from stars with a given age and metallicity (Cid Fernandes et al. 2004).

According to Cid Fernandes et al. (2005), we derived the light-weighted average age $\langle \log t^* \rangle_L$ and the mass-weighted average age $\langle \log t^* \rangle_M$, which are defined as:

$$\langle \log t^* \rangle_L = \sum_{j=1}^N x_j \log t_j \quad \text{and} \quad \langle \log t^* \rangle_M = \sum_{j=1}^N \mu_j \log t_j \quad (3)$$

respectively, where x_j is the modelled light-fraction population vector, and μ_j is the mass-fraction population vector obtained by using the model light-to-mass ratios. By definition, the two weighted average ages are sensitive to different stellar populations: $\langle \log t^* \rangle_L$ is sensitive to the presence of young stellar populations, while $\langle \log t^* \rangle_M$ is sensitive

² <http://www.astro.ufsc.br/starlightst>

³ throughout the paper we use the convention $S_{\nu} \sim \nu^{\alpha}$

to the less luminous and older stellar populations. In Figures 4 and 5, we compared the average ages $\langle \log t^* \rangle_L$ and $\langle \log t^* \rangle_M$ of the restarting radio galaxies and the comparison sample of typical FR II radio galaxies. The observed distribution of the light-weighted age is slightly different for the restarting radio galaxies and FR IIs. The $\langle \log t^* \rangle_L$ distribution for restarting radio galaxies peaks in the range 9.7 – 9.8, as for the comparison sample, but there is a large fraction of younger stellar populations as well. The Kolmogorov-Smirnov two-sample test (K–S test) was performed to check whether the two samples reveal the same distribution. We obtained the probability value $p=0.001$, indicating that the sample of restarting radio sources and the comparison sample have statistically different distributions of $\langle \log t^* \rangle_L$. In the case of mass-weighted age, the observed distributions are similar. The K–S test for $\langle \log t^* \rangle_M$ returns a probability of 0.17 that the restarting and comparison sample radio sources have indistinguishable distributions. The results indicate that while the stellar populations in the restarting radio galaxies do include old stars, similarly as in the FR II radio galaxies, they also show a considerable amount of young stars.

In Figures 6 and 7 we plotted the galaxy mass M^* (the mass of stars obtained with STARLIGHT modelling) as a function of the BH mass and the 1.4 GHz radio luminosity, respectively. It can be seen that the restarting radio galaxies have lower masses of the host galaxy when compared with the FR II radio sources. This may suggest that a larger fraction of galaxy mass in restarting sources is cumulated in gas and/or dust. Since in elliptical galaxies the amount of gas and dust is not significant when compared to spiral galaxies, its presence can be an evidence of merger events occurring in the host galaxies of sources with restarting jet activity.

A very useful parameter for morphological classification of galaxies is the concentration index CI, defined as the ratio of two radii R_{90}/R_{50} , where R_{90} and R_{50} are the radii enclosing 90% and 50% of the r-band Petrosian flux, respectively. According to Nakamura et al. (2003), the CI value lower than 2.86 corresponds to late type galaxies and CI of more than 2.86 – to the early-type galaxies. In Figure 8 we present the distribution of concentration index for the samples of restarting and FR II radio galaxies. It can be seen that the radio sources with recurrent activity tend to have smaller CI values than the radio galaxies from the comparison sample. The difference in distribution of CI indices for restarting and comparison sample radio sources is statistically significant. The K–S test returns a probability of 0.00004 with the maximal deviation between cumulative distributions of 0.34, which indicates that the two considered samples come from different distributions. This can suggest that recurrent activity is observed more often in disturbed/amorphous galaxies.

Moreover, in almost all (~89%) the available spectra of restarting radio sources the emission lines were visible. Using our measurements of the line flux we constructed a diagnostic diagram proposed by Baldwin et al. (1981) and plotted the ratios $[\text{OIII}]/\text{H}\beta$ and $[\text{NII}]/\text{H}\alpha$. In Figure 9 we present diagnostic diagrams for the recurrent radio sources and the comparison sample of FR II galaxies. The diagram used only emission lines with the signal-to-noise ratio of $S/N > 3$. There are 11 sources having $[\text{OIII}]/\text{H}\beta > 3$ in our sample, which represents a high ionisation level. The mean value of the $[\text{OIII}]/\text{H}\beta$ ratio for these sources is very high (~6.6).

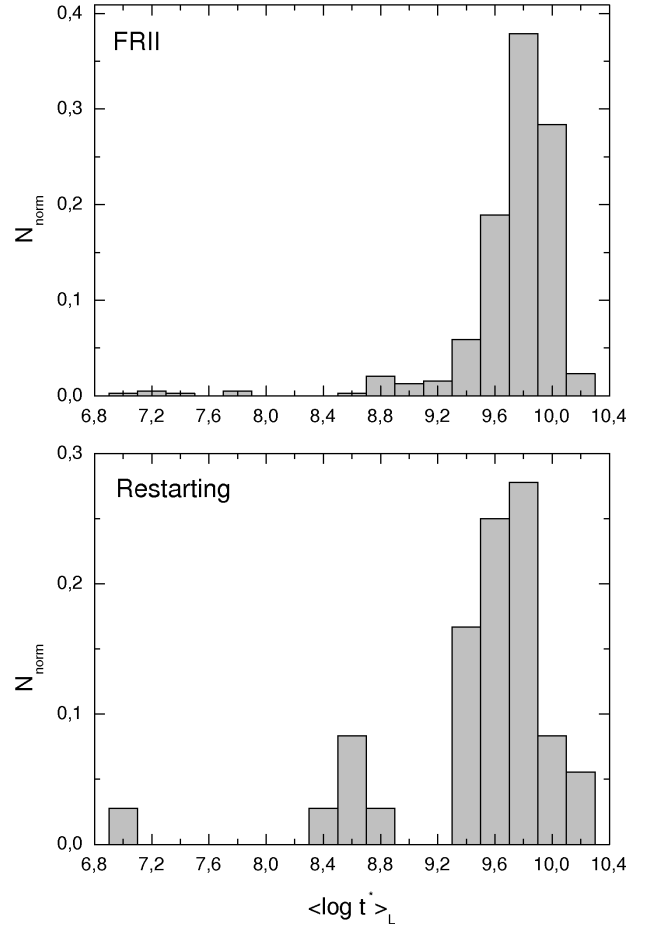


Figure 4. Distribution of light-weighted average age for all 35 restarting radio galaxies for which spectroscopic data are available (*bottom panel*), and single-cycle FR II radio galaxies (*top panel*). The normalised number, N_{norm} , is a number of radio galaxies in a particular bin divided by the total number of sources in the entire sample.

The remaining galaxies have lower $[\text{OIII}]/\text{H}\beta$ ratios with the mean value of 2.1. The restarting radio galaxies are located in the same area on the diagram as the FR II sources, which can suggest that the host galaxies of both types of radio sources are similar. There are no restarting radio sources near the solid line in Figure 9 separating the H II galaxies from AGNs. According to Stasińska et al. (2006), the objects lying away from this line have emission lines excited mostly by an AGN source. There are also no objects in the bottom part of the diagram, where the retired galaxies, i.e. galaxies that have ceased forming stars and are ionized only by their old stellar populations (Stasińska et al. 2015), are located.

We also checked the relation between the radio luminosity and the luminosity of the $[\text{OIII}]$ emission line. It was postulated by Rawlings et al. (1989) and Baum et al. (1988) that the positive correlation can be an evidence for the physical coupling of processes that supply energy both to the emission line regions and to the extended radio structure. The correlations between optical and radio properties are generally explained by the illumination model in which the gas

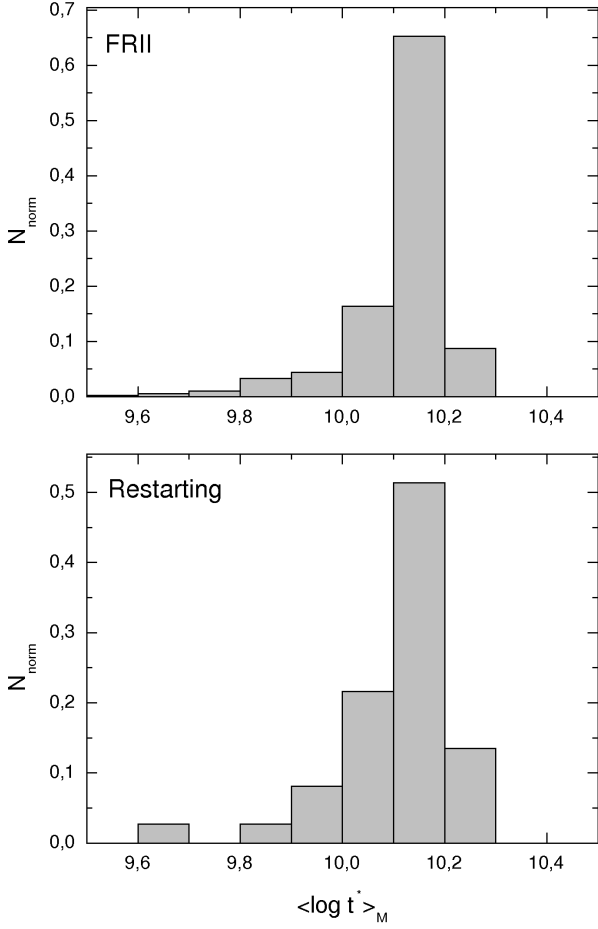


Figure 5. Distribution of mass-weighted average age for restarting radio galaxies (*bottom panel*), and for single-cycle FR II radio galaxies (*top panel*).

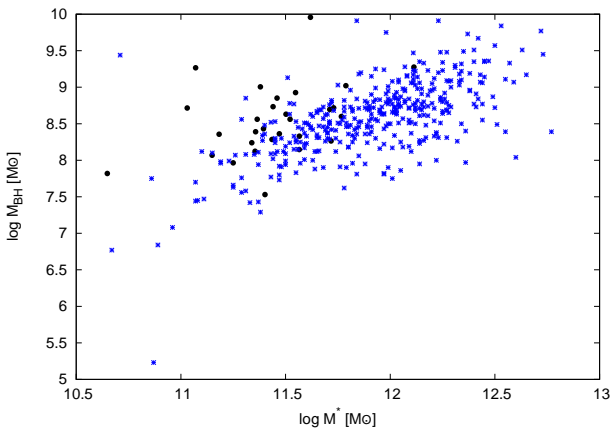


Figure 6. BH mass M_{BH} versus galaxy mass M^* . The restarting radio galaxies are denoted as black dots and the FR II radio galaxies from the comparison sample as blue asterisks.

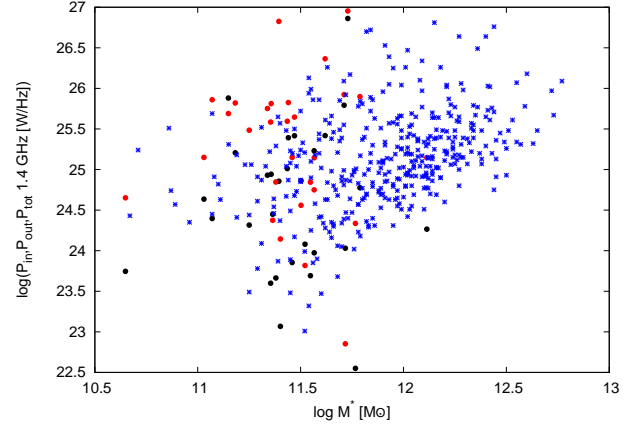


Figure 7. Relation between radio luminosity and the galaxy masses M^* of the restarting and FR II galaxies. The inner radio structures are marked as black dots, the outer structures as red dots, and the FR II radio galaxies from the comparison sample are marked as blue stars. This labelling is used throughout further all similar figures in this paper.

responsible for line emission is photoionized by UV photons coming from the central AGN. We plotted radio luminosity (separately for the inner and outer radio lobes) against the luminosity of the [OIII] emission line. The P–L[OIII] relation is shown in Figure 10. The linear fits to the data points are given by the following relations:

$$\log L_{[\text{OIII}]} = (0.50 \pm 0.14) \cdot \log P_{in} - (4.87 \pm 3.36) \quad (4)$$

$$\log L_{[\text{OIII}]} = (0.57 \pm 0.14) \cdot \log P_{out} - (7.03 \pm 3.62) \quad (5)$$

and for the comparison sample:

$$\log L_{[\text{OIII}]} = (0.93 \pm 0.08) \cdot \log P_{tot} - (16.6 \pm 2.1) \quad (6)$$

The correlation coefficients for the inner radio structure, outer radio structure and the comparison sample are 0.54, 0.58 and 0.68, respectively. For the H_α line we obtained the following relations:

$$\log L_{H_\alpha} = (0.38 \pm 0.12) \cdot \log P_{in} - (2.05 \pm 2.99) \quad (7)$$

$$\log L_{H_\alpha} = (0.46 \pm 0.13) \cdot \log P_{out} - (4.29 \pm 3.27) \quad (8)$$

and for comparison sample:

$$\log L_{H_\alpha} = (0.80 \pm 0.06) \cdot \log P_{tot} - (13.4 \pm 1.7) \quad (9)$$

The correlation coefficients for the inner radio structure, the outer radio structure and the comparison sample are 0.53, 0.59 and 0.73, respectively. The slopes of the fitted lines of the inner and outer radio lobes are slightly flatter than those obtained for the FR II radio galaxies.

4.2 Radio properties

In Figure 12 we plotted the luminosity–linear size relation (P–D diagram) for the sample of restarting and single-cycle FR II radio sources. Most restarting radio sources occupy the same region as the sources from the comparison sample. It can be also observed that the outer doubles tend to be larger

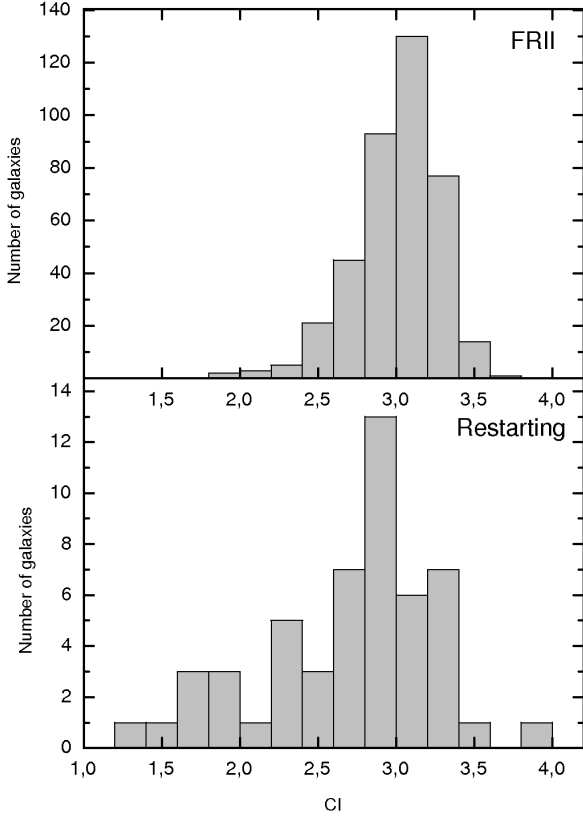


Figure 8. Distribution of concentration indices (CIs) for the restarting radio sources and the comparison sample.

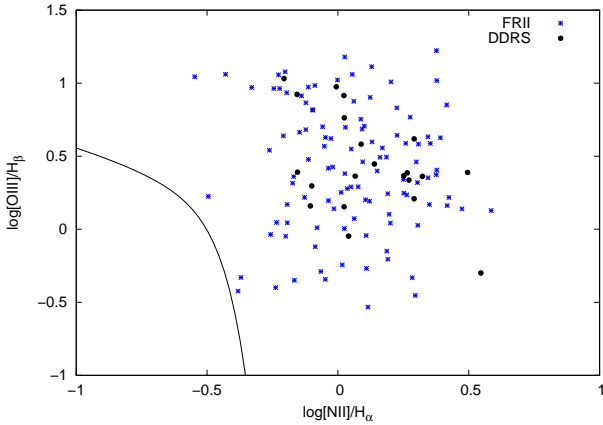


Figure 9. Diagnostic diagram: $[\text{OIII}]/H_{\beta}$ vs. $[\text{NII}]/H_{\alpha}$ for restarting radio galaxies (black dots) and FR II comparison sample (blue asterisks). The solid line indicates the division between AGNs and star-forming galaxies according to [Stasińska et al. \(2006\)](#). In plotting the diagram we used only emission lines with $S/N > 3$.

than the lobes of FR II radio galaxies. This could be an observational bias resulting from the fact that it is easier to detect restarting radio sources of larger size. On the P–D diagram there are also few very compact ($D < 1 \text{ kpc}$) restarting radio sources with high radio luminosities ($\log P > 26 [\text{W/Hz}]$). According to the dynamical and luminosity evolution models of

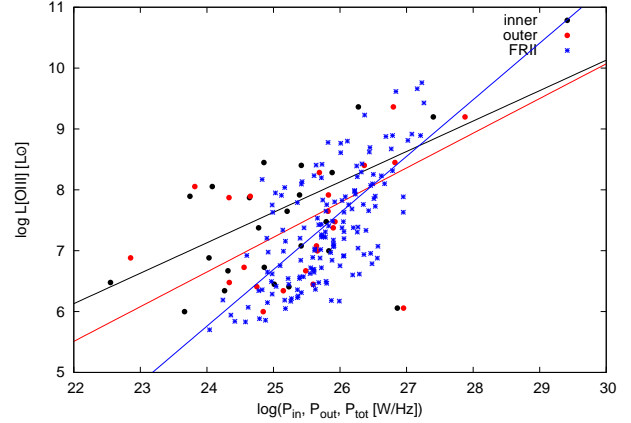


Figure 10. Radio luminosity at 1.4 GHz versus $[\text{OIII}]5007$ line luminosity. For the restarting radio sources the radio luminosities of inner (black dots) and outer (red dots) radio lobes are plotted, while for the comparison sample (blue asterisks) the total radio luminosities are shown. The black and red line corresponds to the best fit for inner and outer radio lobes respectively, while the blue line corresponds to the best fit obtained for the FR II radio galaxies by [Kozieł-Wierzbowska & Stasińska \(2011\)](#).

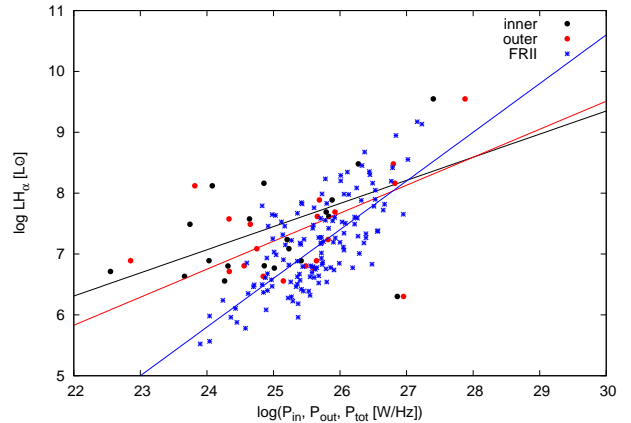


Figure 11. Radio luminosity at 1.4 GHz versus H_{α} line luminosity. The symbols are as in Figure 10.

radio galaxies, three distinct evolutionary phases are to be expected. In the first one, when the lobes are still expanding within the host galaxy, the radio luminosity increases with the source size, which stops as soon as the synchrotron losses become dominant (at the size of about 1 kpc). Beyond this point, the radio luminosity steadily decreases with the increasing source size (up to $\sim 100 \text{ kpc}$) and finally enters the phase of sharply decreasing of luminosity when the inverse Compton losses, resulting from the CMB energy density, dominate the synchrotron losses ([Kaiser & Best 2007](#), [An & Baan 2012](#)).

As shown in Figure 13, there is a significant correlation between luminosity of the outer and inner lobes. The correlation coefficient of a linear fit is 0.59. In our sample of restarting radio galaxies we found 14 sources,

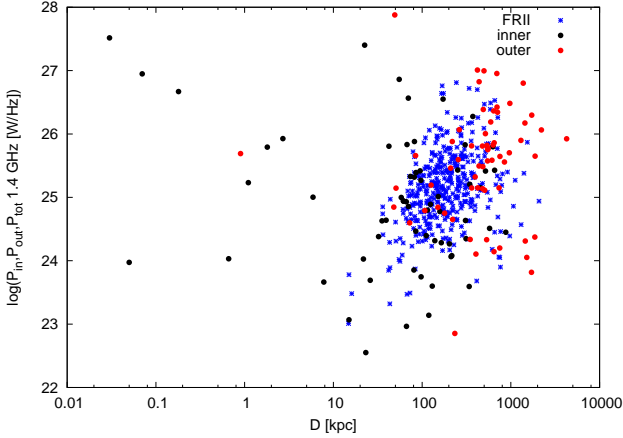


Figure 12. Luminosity–linear size diagrams. For the comparison sample we used total radio luminosity and for the restarting sources we plotted luminosity both for the inner (P_{in}) and the outer (P_{out}) structures.

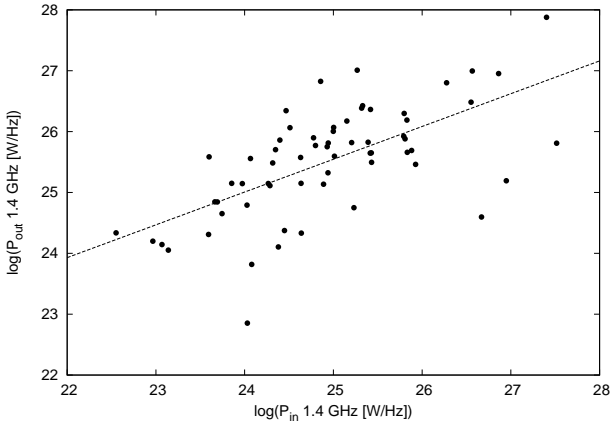


Figure 13. Relation between 1.4 GHz radio luminosity of the inner and the outer radio lobes.

whose inner lobes are more luminous than the outer lobes (i.e. J0041+3224, J0111+3906, J0301+3512, J0301+3512, J0741+3112, J0821+2117, J0840+2949, J0910+0345, J0914+1006, J0943–0819, J1021+1216, J1247+6723 J1352+3126 and J1844+4533). This group of sources is very peculiar and we denoted them by an asterisk in Table 1. Most of them have very compact inner radio structures, but some sources have larger inner lobes (over 100 kpc). It can also be seen that the smaller is the ratio of luminosities ($\log P_{out}/\log P_{in}$), the smaller inner radio structure is observed (in log scales; Fig. 14). Such a trend is found particularly for the luminosity ratios of less than one. For these sources we obtained positive correlation with a coefficient equal to 0.73. The higher luminosity of the inner lobes when compared to that of the outer lobes is explained by Saikia et al. (2006) as a result of more efficient radio emission in the early phase of evolution of the inner lobes when they expand within a dense interstellar medium. As the source expands and traverses a more

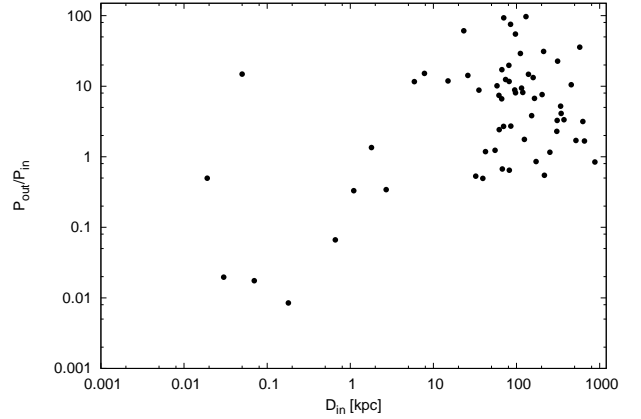


Figure 14. Ratio of 1.4 GHz radio luminosity of outer and inner lobes against the projected linear size of inner radio lobes. The correlation coefficient is $R=0.54$.

diluted medium, the ratio P_{out}/P_{in} usually increases with the size of inner lobes before approaching values of the order of unity. Schoenmakers et al. (2000) postulated the inverse correlation between P_{out}/P_{in} and D_{in} (basing on studies of 7 DDRSs that have the inner doubles larger than 90 kpc). Our results do not confirm this trend but are in agreement with the results obtained by Saikia et al. (2006), who found that $P_{out}/P_{in} < 1$ in the smallest (<1 kpc) inner doubles. They also concluded that the inverse correlation postulated by Schoenmakers et al. (2000) has a reduced level of significance. According to Nandi & Saikia (2012), there could be only an upper envelope to this diagram, suggesting an inverse relation. The small number of sources on the left side of Figure 14 can be caused by the selection effects. Resolving very compact inner doubles that are smaller than 10 kpc is possible only with high-resolution radio observations. Furthermore, we also found that nearly half of the restarting radio galaxies have brighter inner and outer radio lobes on the same side of the host galaxy (i.e. out of 41 radio galaxies for which the inner and outer lobes are well detached, the brighter inner and outer lobes are on the same side in 18 galaxies, and 23 galaxies show brighter inner and outer lobes on the opposite sides of the host galaxy). A similar trend is observed, when the length of the radio lobes is considered – 22 and 19 sources, respectively. These findings can be explained as resulting from the combination of orientation of a radio source and an activity intermission to have occurred between the active periods. Only in an ideal case of symmetric jets and isotropic properties of the ambient medium, one could expect the same radio luminosity and equal lengths of both lobes. In reality, the orientation of radio sources in space is random and only some of them are aligned in the sky plane. Due to the latter, we expect Doppler effects to be responsible for the brightness differences. Moreover, the light-travel time effect, consisting in that radiation from the far-side lobe arrives at the observer significantly later due to its longer distance than from the near-side lobe, should be taken into account (see Marecki 2012).

In Figure 15 we plotted the radio luminosity against the mass of the black hole. The distribution of sources in

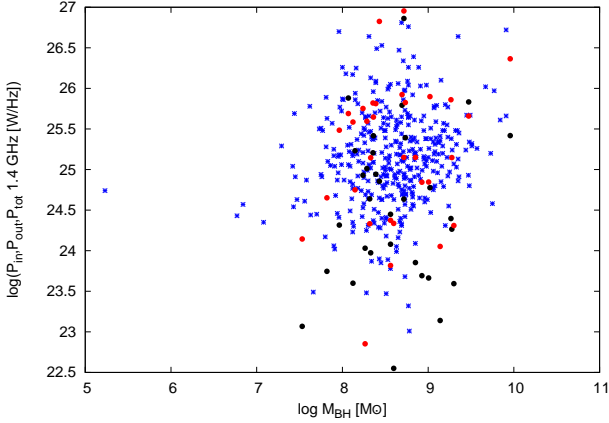


Figure 15. Relation between BH mass and radio luminosity at 1.4 GHz.

the P - M_{BH} plane is much similar for both the samples. We also compared the distributions of the black hole mass for the FR II sample, restarting radio galaxies sample, and X-shaped radio sources studied by Mezcua et al. (2011, 2012). All the distributions are presented in Figure 16. In the case of FR II radio galaxies, the distribution of the black hole mass is very symmetric with a peak value of $\log(M_{\text{BH}}/M_{\odot})$ ranging from 8.6 to 8.8 and the median value of 8.58. For the restarting radio galaxies the M_{BH} distribution does not have any pronounced maximum. However, the median value of $\log(M_{\text{BH}}/M_{\odot})$ is 8.61, much the same as those of typical FR II sources. The distribution for the X-shaped radio galaxies is nearly symmetric around the peak value, which is similar to the one of the restarting radio sources. The median value of $\log(M_{\text{BH}}/M_{\odot})$ for the X-shaped galaxies of ~ 8.3 is smaller than for the other two samples.

4.3 Infrared properties

Almost all the recurrent activity radio galaxies discussed in this paper were detected by the Wide-Field Infrared Survey Explorer (WISE; Wright et al. 2010). In Figure 17 we plotted the colour-colour diagram, where the vertical axis W1-W2 corresponds to the magnitude difference between the 3.4 and the 4.6 μm bands and the horizontal axis W2-W3 corresponds to the magnitude difference between the 4.6 and the 12 μm bands. We plotted the WISE colours only for 49 restarting and 388 FR II radio sources, for which all magnitudes were above the detection limit. In Figure 17 we marked our sources in the diagram showing the regions where the different classes of the WISE-detected sources are located (Wright et al. 2010). The vertical dotted line, which, according to Wright et al. (2010), divides elliptical and spiral galaxies, has a WISE W2-W3 colour value of +1.5 magnitude. The most powerful AGNs lie above the W1-W2 colour level of +0.6 magnitude. It can be clearly seen that most of the restarting radio sources (67%) are located in the regions where spiral galaxies, being typically ISM-abundant, reside. In the comparison sample less than half (41%) of FR II radio sources are in that region. Also most of the studied radio sources have W1-W2 colours lower than 0.5 and

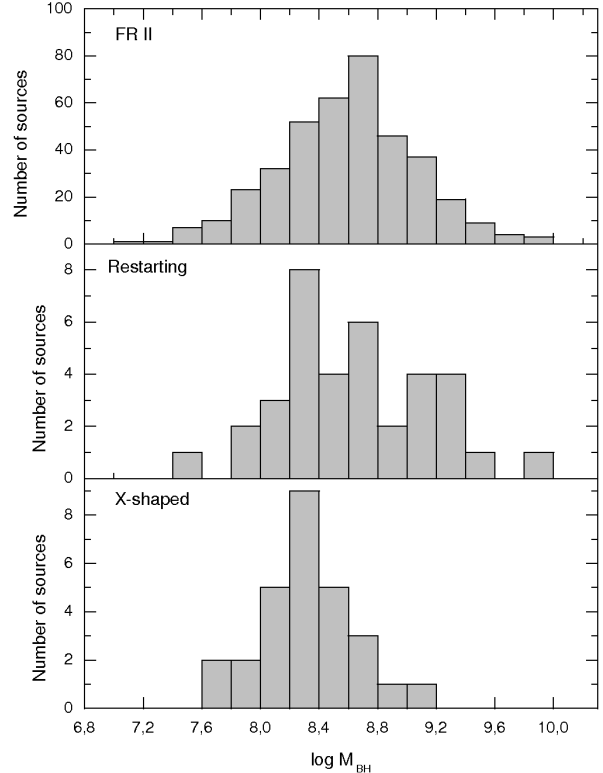


Figure 16. BH mass distribution for FR II (top panel), restarting radio galaxies (middle panel) and X-shaped radio sources (bottom panel).

according to Izotov et al. (2014), for galaxies with $W1-W2 < 0.5$ the main source of radiation is the stellar and ionised gas emission. The location of radio sources in this region was explained by Assef et al. (2010) as a consequence of small Eddington ratios. In such galaxies, the mid-infrared colours are not dominated by the AGN, while they are contaminated by the host. Therefore, the colours generally originate from stars and emission from the cold dust of star formation.

5 CONCLUSIONS

We compiled and presented the largest (to date) sample of 74 restarting radio sources, using optical, radio, and infrared data to determine their physical properties and compare them with a sample of typical FR II radio galaxies with single activity. We came to the following conclusions:

- (i) The black hole masses of radio sources with recurrent activity are similar to those observed in FR II radio galaxies.
- (ii) Recurrent and typical radio sources show different compositions of stellar populations. The hosts of restarting radio sources contain a larger amount of young stars.
- (iii) The total mass of stars in the host galaxies of the recurrent activity sources is, on average, less than that in the FR II hosts. The concentration index for the restarting radio sources tends to be slightly lower than that of the FR II sources, which indicates that they can have hosts with more disturbed morphologies. Both the facts could be the evidence that the restarting radio sources are more common in galaxies after mergers.

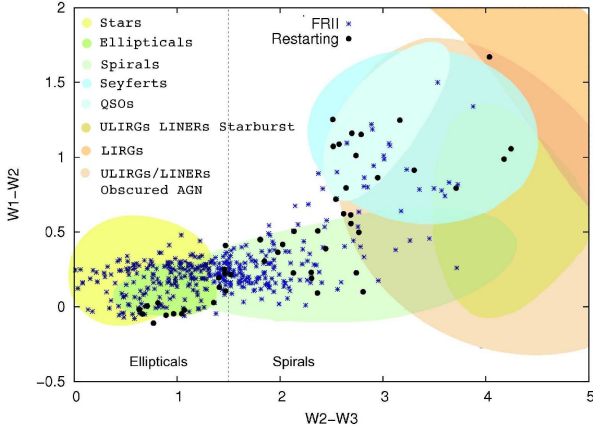


Figure 17. Colour-colour diagram for restarting and FR II radio sources. The coloured areas represent different classes of sources and the dotted line ($W2-W3=1.5$) shows a proposed division between elliptical and spiral galaxies (according to [Wright et al. 2010](#)).

(iv) Emission lines are visible in almost all (89%) the available spectra of recurrent jet activity hosts. Basing on the diagnostic diagram, the emission lines are excited by an AGN-like driven process.

(v) There is a significant correlation between the luminosity of the emission line and the radio luminosity of the inner and outer radio lobes. The correlation is on the same level for the $H\alpha$ as well as for [OIII] line.

(vi) There is a strong correlation between the radio luminosity of the inner and outer lobes.

(vii) In the case of 13 restarting radio galaxies, the inner lobes are more luminous than the outer ones. This can be seen not only in very compact ($<1\text{kpc}$) inner doubles, but in much more extended ones as well, with linear sizes of few hundred kiloparsecs.

(viii) Almost half of restarting radio sources have brighter/larger inner and outer lobes on the opposite sides of host galaxy.

(ix) The infrared WISE colour-colour diagram shows that the 67% hosts of recurrent jet activity radio galaxies reside in the region typical for spiral galaxies or other dusty, late-type galaxies with some ongoing star formation, while only 41% of FR II radio sources are found in that region.

ACKNOWLEDGEMENTS

We thank the anonymous referee for her/his very valuable comments. The work is supported by Polish NSC grant DEC-2013/09/B/ST9/00599.

REFERENCES

Ahn C.P., et al., 2014, *ApJS*, 211, 17
 An T., Baan W. A., 2012, *ApJ*, 760, 77
 Assef R. J., et al., 2010, *ApJ*, 713, 970
 Baade W., Minkowski R., 1954, *ApJ*, 119, 206
 Bagchi J., et al., 2014, *ApJ*, 788, 174
 Baldwin J. A., Phillips M. M., Terlevich R., 1981, *PASP*, 93, 5

Baum S. A., O’Dea C. P., Murphy D. W., de Bruyn A. G., 1990, *A&A*, 232, 19
 Baum S. A., Heckman T., Bridle A. H., van Breugel W., Miley G., 1988, *ApJS*, 68, 643
 Becker R. H., White R. L., Helfand D. J., 1995, *ApJ*, 450, 559
 Black A. R. S., Baum S. A., Leahy J. P., Perley R. A., Riley J. M., Scheuer P. A. G., 1992, *MNRAS*, 256, 186
 Blundell K. M., Fabian A. C., 2011, *MNRAS*, 412, 705
 Bondi M., Marchã M. J. M., Polatidis A., Dallacasa D., Stanghellini C., Antón S., 2004, *MNRAS*, 352, 112
 Bridle A. H., Fomalont E. B., Cornwell, T. J., 1981, *AJ*, 86, 1294
 Bridle A. H., Perley R. A., Henriksen R. N., 1986, *AJ*, 92, 534
 Brocksopp C., Kaiser C. R., Schoenmakers A. P., de Bruyn A. G., 2007, *MNRAS*, 382, 1019
 Brocksopp, C., Kaiser, C. R., Schoenmakers, A.P., de Bruyn, A. G., 2011, *MNRAS*, 410, 484
 Brown M. J. I., Webster R. L., Boyle B. J., 2001, *AJ*, 121, 2381
 Bruzual G., Charlot S., 2003, *MNRAS*, 344, 1000
 Burns J. O., Christiansen W. A., Hough D. H., 1982, *ApJ*, 257, 538
 Burns J.O., Feigelson E. D., Schreier E.J., 1983, *ApJ*, 273, 128
 Buttiglione S., Capetti A., Celotti A., Axon D.J., Chiaberge M., Macchetto F.D., Sparks W.B., 2009, *A&A*, 495, 1033
 Cid Fernandes R., Gu Q., Melnick J., Terlevich E., Terlevich R., Kunth D., Rodrigues L.R., Joguët B., 2004, *MNRAS*, 355, 273
 Cid Fernandes R., Mateus A., Sodré L., Stasińska G., Gomes J. M., 2005, *MNRAS*, 358, 363
 Clarke D. A., Bridle A. H., Burns J. O., Perley R. A., Norman M. L., 1992, *ApJ*, 385, 173
 Clarke D. A., Burns J. O., Norman M. L., 1992b, *ApJ*, 395, 444
 Colafrancesco S., Marchegiani P., de Bernardis P., Masi S., 2013, *A&A*, 550, 92
 Condon J. J., Cotton W. D., Greisen E. W., Yin Q. F., Perley R. A., Taylor G. B., Broderick J. J., 1998, *AJ*, 115, 1693
 Czerny B., Siemiginowska A., Janiuk A., Nikiel-Wroczyński B., Stawarz L., 2009, *ApJ*, 698, 840
 Ellingson S. W., Clarke T. E., Cohen A. et al., 2009, *IEEEEP*, 97, 1421
 Fanaroff B. L., Riley J. M., 1974, *MNRAS*, 167, 31
 Ferrarese L., Merritt D., 2000, *ApJ*, 539, 9
 Ge J., Owen F. N., 1994, *AJ*, 108, 1523
 Gebhardt K., et al., 2000, *ApJ*, 539, 13
 Giovannini G., Taylor G. B., Feretti L., Cotton W. D., Lara L., Venturi T., 2005, *ApJ*, 618, 635
 Graham A. W., et al., 2011, *MNRAS*, 412, 2211
 Ho L. C., Filippenko A. V., Sargent W. L., 1995, *ApJS*, 98, 477
 Hota A., et al., 2011, *MNRAS*, 417L, 36
 Izotov Y.I., Guseva N.G., Fricke K.J., Henkel C., 2014, *A&A*, 561, 33
 Jamrozny M., Konar C., Saikia D. J., Stawarz L., Mack K. H., Siemiginowska A., 2007, *MNRAS*, 378, 581
 Jamrozny M., Saikia D. J., Konar C., 2009, *MNRAS*, 399L, 141
 Kaiser C. R., 2000, *A&A*, 362, 447
 Kaiser C. R., Best P. N., 2007, *MNRAS*, 381, 1548
 Kellermann K.I., Owen F.N., 1988, in Kellermann K.I., Verschuur G.L., eds, *Galactic and extragalactic radio astronomy*, 2nd edn, Springer Verlag, Berlin, p. 563
 Konar C., Hardcastle M. J., Jamrozny M., Croston J. H., 2013, *MNRAS*, 430, 2137
 Konar C., Saikia D. J., Jamrozny M., Machalski J., 2006, *MNRAS*, 372, 693
 Koziel-Wierzbowska D., Stasińska G., 2011, *MNRAS*, 415, 1013
 Koziel-Wierzbowska D., Jamrozny M., Zola S., Stachowski G., Kuźmicz A., 2012, *MNRAS*, 422, 1546
 Kronberg P. P., Wielebinski R., Graham D. A. 1986, *A&A*, 169, 63
 Leahy J. P., Black A. R. S., Dennett-Thorpe J., Hardcastle M. J.,

- Komissarov S., Perley R. A., Riley J. M., Scheuer P. A. G., 1997, *MNRAS*, 291, 20
- Leahy J. P., Perley R. A., 1991, *AJ*, 102, 537
- Liu F. K., 2004, *MNRAS*, 347, 1357
- Liu F. K., Wang D., Chen X., 2012 *ApJ*, 746, 176
- Liu F. K., Wu X.-B., Cao S. L., 2003, *MNRAS*, 340, 411
- Lonsdale C. J., Cappallo R. J., Morales M. F., 2009, *IEEEEP*, 97, 1497
- Machalski J., Jamrozy M., Zoła S., KozielD., 2006, *A&A*, 454, 85
- Machalski J., Koziel-Wierzbowska D., Jamrozy M., 2007, *AcA*, 57, 227
- Marecki A., Barthel P. D., Polatidis A., Owsianik I., 2003, *PASA*, 20, 16
- Marecki A., Jamrozy M., Machalski J., 2016, *MNRAS*, 463, 338
- Marecki A., Szablewski 2009, *A&A*, 506L, 33
- Marecki A., 2012, *A&A*, 544L, 2
- Merritt D., Ekers R. D., 2002, *Science*, 297, 1310
- Mezcua M., Lobanov A. P., Chavushyan V. H., León-Tavares J., 2011, *A&A* 527, 38
- Mezcua M., Lobanov A. P., Chavushyan V. H., León-Tavares J., 2012, *A&A* 544, 36
- Morganti et al., 1993, *MNRAS*, 263, 1023
- Nakamura O., Fukugita M., Yasuda N., Loveday J., Brinkmann J., Schneider D. P., Shimasaku K., SubbaRao M., 2003, *AJ*, 125, 1682
- Nandi S., Saikia D. J., 2012, *BASI*, 40 121
- Owen F. N., Ledlow M. J., 1997, *ApJS*, 108, 41
- Parma P., Murgia M., Morganti R., Capetti A., de Ruiter H. R., Fanti R., 1999, *A&A*, 344, 7
- Perley R. A., Bridle A. H., Willis A. G., Fomalont E. B., 1980, *AJ*, 85, 499
- Rawlings S., Saunders R., Eales S. A., Mackay C. D., 1989, *MNRAS*, 240, 701
- Roettiger K., Burns J. O., Clarke D. A., Christiansen W. A., 1994, *ApJ*, 421L, 23
- Safouris V., Subrahmanyam R., Bicknell G. V., Saripalli L., 2008, *MNRAS*, 385, 2117
- Saikia D. J., Jamrozy M., 2009, *BASI*, 37, 63
- Saikia D. J., Konar C., Kulkarni V. K., 2006, *MNRAS*, 366, 1391
- Saripalli L., Subrahmanyam R., 2009, *ApJ*, 695, 156
- Saripalli L., Subrahmanyam R., Udaya Shankar N., 2002, *ApJ*, 565, 256
- Saripalli L., Subrahmanyam R., Udaya Shankar N., 2003, *ApJ*, 590, 181
- Saripalli L., Subrahmanyam R., Thorat K., Ekers R.D., Hunstead R.W., Johnston H.M., Sadler E.M., 2012, *ApJS*, 199, 27
- Saripalli L., Malarecki J. M., Subrahmanyam R., Jones D.H., Staveley-Smith L., 2013, *MNRAS*, 436, 690
- Scheuer P. A. G., 1974, *MNRAS*, 166, 513
- Schilizzi R. T. et al., 2001, *A&A*, 368, 398
- Schoenmakers A. P., de Bruyn A. G., Röttgering H. J. A., van der Laan H., Kaiser C. R., 2000, *MNRAS*, 315, 371
- Siemiginowska A., et al., 2003, *ApJ*, 595, 643
- Sikora M., Stasińska G., Koziel-Wierzbowska D., Madejski G.M., Asari N.V., 2013, *ApJ*, 765, 62S
- Shen Y., Greene J. E., Strauss M. A., Richards G. T., Schneider D. P., 2008, *ApJ*, 680, 169
- Shulevski A., Morganti R., Oosterloo T., Struve C., 2012, *A&A*, 545, 91
- Shulevski A., 2015, PhD Thesis, Univ. of Groningen
- Stanghellini C., O'Dea C. P., Dallacasa D., Cassaro P., Baum S. A., Fanti R., Fanti C., 2005, *A&A*, 443, 891
- Stasińska G., Cid Fernandes R., Mateus A., Sodré L., Asari N. V., 2006, *MNRAS*, 371, 972
- Stasińska G., Costa-Duarte M.V., Vale Asari N., Cid Fernandes R., Sodré L., 2015, *MNRAS*, 449, 559
- Strom R. G., Willis A. G., 1980, *A&A*, 85, 36
- Strateva I., et al., 2001, *AJ*, 122, 1861
- Subrahmanyam R., Saripalli L., Hunstead R. W., 1996, *MNRAS*, 279, 257
- Valtonen M. J., et al., 2008, *Nature*, 452, 851
- van Breugel W., Fomalont E. B., 1984, *ApJ*, 282L, 55
- van Haarlem M. P. et al., 2013, *A&A*, 556, 2
- Venturi T., Dallacasa D., Stefanachi F., 2004, *A&A*, 422, 515
- Wagner A. Y., Bicknell G. V., 2011, *ApJ*, 728, 29
- Willis A. G., Strom R. G., Wilson A. S., 1974, *Nature*, 250, 625
- Wright E. L., et al., 2010, *AJ*, 140, 1868
- Zhao J. H., Sumi D. M., Burns J. O., Duric N., 1993, *ApJ*, 416, 51

Table 1: Radio sources with evidence of recurrent activity.

Source Name (1)	IAU Name (2)	REC _{12000.0} h m s (3)	DEC _{12000.0} ° ' " (4)	Opt. Id. (5)	Red-shift (6)	l_{in} kpc (7)	l_{in} arcsec (8)	l_{out} kpc (9)	l_{out} arcsec (10)	S_{in} mJy (11)	S_{out} mJy (12)	$\log M_{BH}$ M_{\odot} (13)	Class A/B (14)	Ref. Cmt. (15)
J0009+1244	4C12.03	00 09 52.60	+12 44 04.64	G	0.156	114.9	43	553.1	207	100	907	-	A	1,f
J0037+1319	3C16	00 37 44.57	+13 19 55.00	G	0.405	96.91	18	419.9	78	35	1765	-	A	1,2
J0041+3224*		00 41 46.12	+32 24 52.65	G	(0.45)	172	30	974	170	525	409	-	A	3
J0042-0613		00 42 46.85	-06 13 52.92	G	0.123	518.1	237.1	753.6	344.9	690	1140	9.23	A	4,a,e
J0104-6609		01 04 21.26	-66 09 17.30	G	(1.19)	66.7	8	750	90	0.37	5.22	-	A	5
J0111+3906*	B0108+388	01 11 37.32	+39 06 28.10	G	0.6685	0.07	0.01	126.1	18	519	8	-	B?	6,b,c
J0116-4722		01 16 25.04	-47 22 41.60	G	0.146	455	180	1441	570	260	2640	-	A	7
J0301+3512*	4C 34.09	03 01 42.37	+35 12 20.68	G	0.0165	0.66	2	233.7	706	1800	119	8.26	B	2,i
J0301+3550*	4C 35.06	03 01 51.50	+35 50 30.00	G	0.0463	32.29	36	403.7	450	492	258	-	A	8
J0303+1626	3C76.1	03 03 15.02	+16 26 19.06	G	0.0325	21.8	34.1	107.1	167.4	450.2	2602	-	B	1
J0351-2744	PKS0349-27	03 51 35.76	-27 44 34.70	G	0.0662	251.8	200.8	437.8	349.1	2636	3009	-	A	9
J0504+3806	3C134	05 04 42.19	+38 06 11.40	G	-	-	115.6	-	166.1	1485	7862	-	A	a
J0709-3601	PKS0707-35	07 09 14.09	-36 01 21.80	G	0.218	627.1	179.4	1720	492	480	1444	-	A	10,11
J0741+3112*	B2 0738+31	07 41 10.70	+31 12 00.22	Q	0.632	0.03	0.005	478.5	70	2188	38	9.37	A	12,b,h
J0746+4526		07 46 17.92	+45 26 34.46	G	0.5502	95	15.2	640	100.1	24.2	191.6	9.96	A	13
J0804+5809		08 04 42.79	+58 09 34.94	S	-	-	21.6	-	106.3	58.6	192.1	-	A	13
J0821+2117*	B0818+214	08 21 07.50	+21 17 02.87	G	0.418	2.7	0.5	209.8	38.24	148	46.4	-	A	14
J0840+2949*	4C29.30	08 40 02.36	+29 49 02.63	G	0.0647	39.3	32	533.3	434.6	446.7	216.9	8.32	B	15
J0847+3147	IC2402	08 47 59.04	+31 47 08.37	G	0.0674	203	159.3	362.1	284.2	173.9	1303	9.28	A	16
J0855+4204		08 55 49.15	+42 04 20.11	G	(0.279)	35.3	8.4	545.9	130	18.8	155.7	-	A	13
J0910+0345*		09 10 59.10	+03 45 31.68	G	(0.588)	42.3	6.4	218.8	33.1	50.7	53.4	-	A	13
J0914+1006*		09 14 19.53	+10 06 40.59	G	0.308	216.2	48	1709	379.7	252.5	129.1	8.56	A	a
J0921+4538	3C219	09 21 08.61	+45 38 57.36	G	0.174	70.1	24	438.5	150	90	8046	8.43	A	17,18,19
J0924+0602		09 24 49.04	+06 02 42.80	G	0.231	80.8	22.1	424	116	4.8	90	8.85	A	a
J0927+2932		09 27 44.88	+29 32 32.30	S	-	-	24	-	115	19	17	-	A	8
J0927+3510		09 27 50.59	+35 10 50.73	G	(0.55)	575.5	90	2206	345	3	96	-	A	20
J0929+4146		09 29 10.66	+41 46 45.59	G	0.365	655.6	130	1876	372	64	99	-	A	21,d,g
J0935+0204	4C02.27	09 35 18.19	+02 04 15.54	Q	0.6491	69.9	10.1	498	71.96	230.3	547.6	9.56	A	22
J0943-0819*	B0941-080	09 43 36.94	-08 19 30.81	G	0.228	0.18	0.05	72.34	20	3232	26	-	B?	23,h
J1004+5434		10 04 51.83	+54 34 04.29	G	0.047	55.2	60.6	694.2	762.9	90	110	8.72	A	24,a
J1006+3454		10 06 01.73	+34 54 10.52	G	0.101	1.8	1	4248	2310	2500	3300	8.70	A	25,26,27
J1021+1216*		10 21 24.21	+12 17 05.44	G	0.129	876.4	385	1865	819.4	67.3	55	8.56	A	4,a
J1039+0536		10 39 28.21	+05 36 13.62	G	0.35	81.5	16.6	488.7	99.6	54.9	594.9	-	A	13
J1103+0636		11 03 13.29	+06 36 16.00	G	0.4406	66.3	11.7	548.8	96.9	13.2	79.9	8.24	A	13
J1158+2621	4C26.35	11 58 20.13	+26 21 12.07	G	0.112	139	69	483.8	240	67	962	7.96	A	13,28
J1159+5820		11 59 05.68	+58 20 35.57	G	0.054	23.2	22.4	348.2	335.8	5.3	319.1	8.60	A	29
J1208+0821		12 08 56.78	+08 21 38.57	G	0.5841	111.3	16.9	648.9	98.5	2	51.9	9.27	A	13
J1238+1602		12 38 21.20	+16 02 41.42	S	-	-	40.8	-	115.6	8.9	56.5	-	A	13
J1242+3838		12 42 36.82	+38 38 06.15	G	0.408	308.3	57	735.5	136	8	24	8.72	A	30
J1247+6723*		12 47 33.31	+67 23 16.46	G	0.107	0.019	0.01	1196	618	260	126	8.63	A	31,32

Table 1 *continued*

Source Name	IAU Name	REC J2000 (3)	DEC J2000 (4)	Opt. Id. (5)	Redshift (6)	l_{in} kpc (7)	l_{in} arcsec (8)	l_{out} kpc (9)	l_{out} arcsec (10)	S_{in} mJy (11)	S_{out} mJy (12)	$\log M_{BH}$ M_{\odot} (13)	Class A/B (14)	Ref. Comment (15)
J1325-4301	Cen A	13 25 27.62	-43 01 08.81	G	0.0018	21.3	67	266.4'	1800'	$28 \cdot 10^4$	$52 \cdot 10^4$	-	A	33,34
J1326+1924		13 26 13.67	+19 24 23.75	G	0.1762	26	8.8	150.6	51	6	81.8	8.93	A	13
J1328+2752		13 28 48.45	+27 52 27.81	G	0.0911	97.3	58	220.8	131.7	27.9	219.9	7.82	A	13
J1344-0030		13 44 46.92	-00 30 09.31	G	0.5801	85.4	13	631	96.1	20.1	48.7	8.73	A	13
J1352+3126	3C293	13 52 17.88	+31 26 46.49	G	0.045	1.1	1.2	179.5	204.2	3703	1209	8.15	A	35
J1407+5132	4C51.31	14 07 18.48	+51 32 04.63	G	(0.324)	84.8	18.2	707.5	151.8	9.2	646.2	-	A	13
J1409-0302		14 09 48.85	-03 02 32.53	G	0.1378	52.9	22	308	128	4	48	8.61	A	36,d
J1443+5201	3C303	14 43 02.75	+52 01 37.23	G	0.1412	81.9	33.3	90.9	37	1500	935	8.07	B	1
J1453+3308	4C33.33	14 53 02.86	+33 08 42.40	G	0.249	158.5	41	1299	336	34	426	9.02	A	30,37
J1500+1542		15 00 55.18	+15 42 40.56	G	(0.456)	124.2	21.5	480.7	83.2	11.1	17.8	-	A	13
J1504+2600	3C310	15 04 57.12	+26 00 58.46	G	0.0538	152.1	147.1	255.4	247	1547	5846	8.29	B	38
J1513+2607	3C315	15 13 40.05	+26 07 30.46	G	0.1083	5.9	3	262	134	350.2	3967	9.98	A	39,f
J1516+0701	3C317	15 16 44.48	+07 01 17.83	G	0.0345	0.05	0.08	50.85	75	353	5191	8.33	B?	40,41
J1520-0546		15 20 13.29	-05 46 27.01	G	0.0601	118.8	103.7	1513	1320	16.5	132.8	9.14	A	4,a
J1521+5214		15 21 05.90	+52 14 39.91	G	(0.537)	61.9	9.8	396	62	8.5	18.5	-	A	13
J1528+0544		15 28 04.95	+05 44 28.18	G	0.0401	15.0	19.2	645.2	824	32.2	379.3	7.53	A	4,a
J1534+1016		15 34 18.63	+10 16 47.54	G	0.1333	164.6	70.3	507.1	216.6	43	280	-	A	28
J1538-0242		15 38 41.31	-02 42 05.51	G	(0.575)	58.2	8.9	517.1	79.1	8.3	75.2	-	A	13
J1545+5047		15 45 17.20	+50 47 53.94	G	0.4309	61.5	11	361.1	64.6	14.3	96.9	8.39	A	13
J1548-3216		15 48 58.05	-32 16 57.60	G	0.108	312.2	160	961.8	493	78	1722	-	A	42,43
J1604+3438		16 04 45.89	+34 38 16.53	G	0.282	211.6	50	846.4	200	5	146	-	A	20
J1605+0711		16 05 13.74	+07 11 52.56	G	0.3112	344.1	75.9	538.6	118.8	55.3	212.6	8.36	A	13
J1627+2906		16 27 54.63	+29 06 20.01	G	(0.722)	73.8	10.2	697.4	96.4	10.4	112.9	-	A	13
J1628+3933	3C338	16 28 38.24	+39 33 04.55	G	0.0304	7.8	13	48	80	224	3380	9.01	B	7,44
J1649+4133		16 49 28.32	+41 33 41.61	S	-	-	6.7	-	39.7	2.4	39	-	A	13
J1651+0459	3C348	16 51 08.15	+04 59 33.32	G	0.1550	212.6	80	319.5	120.2	-	70.7	9.07	B?	45
J1705+3940		17 05 17.83	+39 40 29.25	G	(0.701)	305.3	42.7	592.7	82.9	35.2	69.3	-	A	13
J1706+4340		17 06 25.44	+43 40 40.16	S	(0.525)	194	31.8	687.2	110.1	79.3	604	-	A	13,46
J1835+6204		18 35 10.92	+62 04 08.14	G	0.519	372.3	60	1378	222	200	604	-	A	30
J1844+4533*	3C388	18 44 02.40	+45 33 29.70	G	0.0917	67.48	40	84.35	50	3362	2205	9.47	B	47,48
J2048+0701	3C424	20 48 12.03	+07 01 17.48	G	0.127	22.5	10	49.2	21.9	625	1816	-	A	49
J2107+2331	4C 23.56	21 07 15.08	+23 31 43.71	G	2.483	457	55.7	492.2	60	-	397	-	A	50
J2223-0206	3C445	22 23 49.54	-02 06 12.90	G	0.056	130	121	612	570	55	5260	8.12	A	51,52
J2345-0449		23 45 32.71	-04 49 25.32	G	0.0757	338.9	238.9	1454	1025	29	148.4	-	A	4,53

Column designation: (1) – source name, (2) – other name, (3), (4) – right ascension and declination (J2000), (5) – optical identification (G – galaxy, Q – quasar, S – unidentified source), (6) – redshift, (7) and (9) – projected linear size of the inner and outer lobes, respectively, (8) and (10) – apparent angular size of the inner and outer lobes respectively, (11) and (12) – flux densities at 1.4 GHz of the inner and outer lobes, respectively, (13) – mass of the central black hole, (14) – class of radio structure (A or B), (15) – references. The redshift given in brackets corresponds to the Sloan Digital Sky Survey (SDSS) photometric redshift. For two objects, J1409-0302 and J1325-4301, we wrote two values of l_{out} and S_{out} , which correspond to the length and flux density of the middle and outer lobes, respectively. The bolded names of

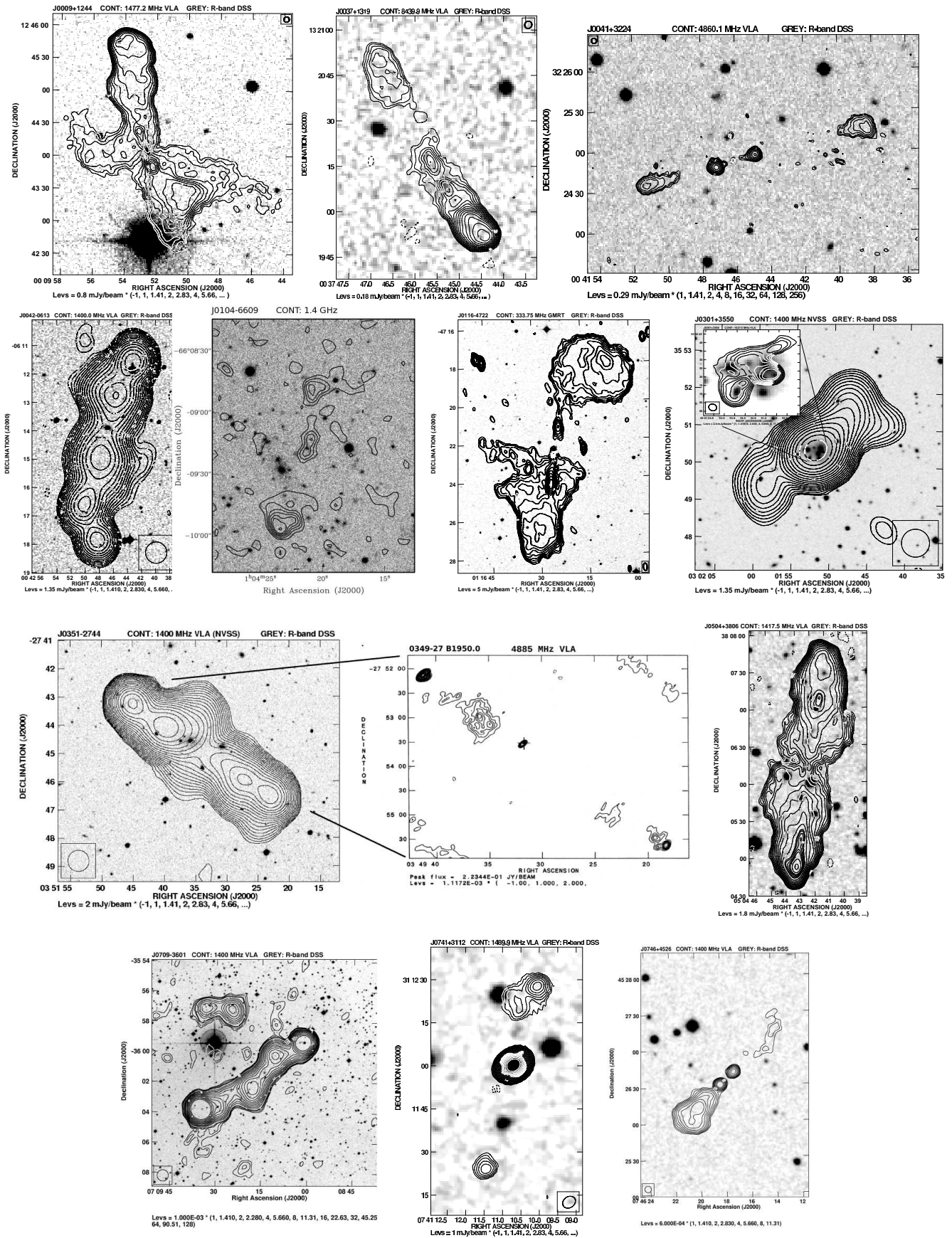
sources correspond to newly recognized restarting radio galaxies.

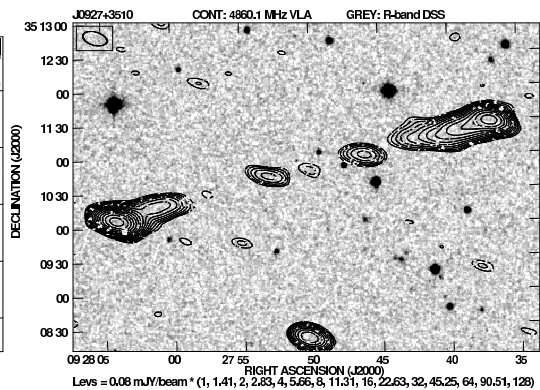
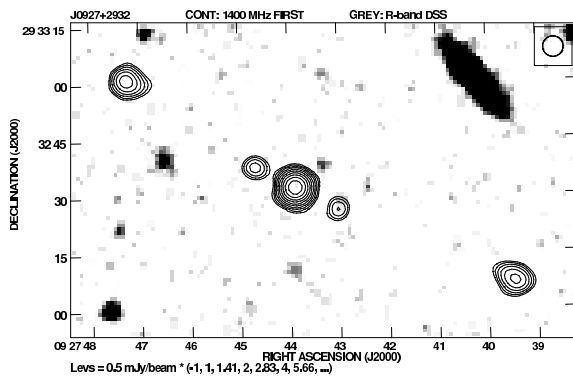
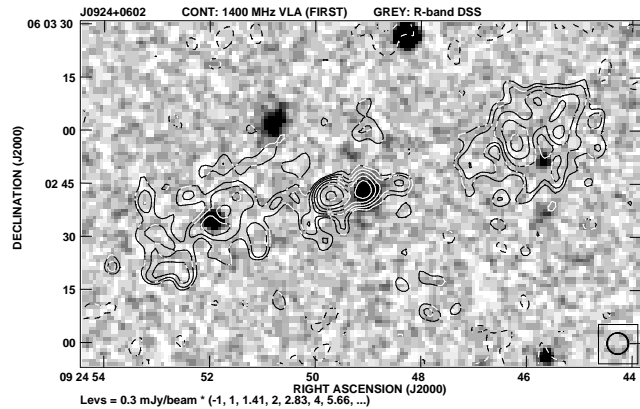
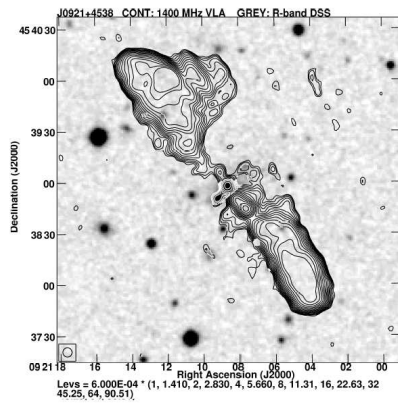
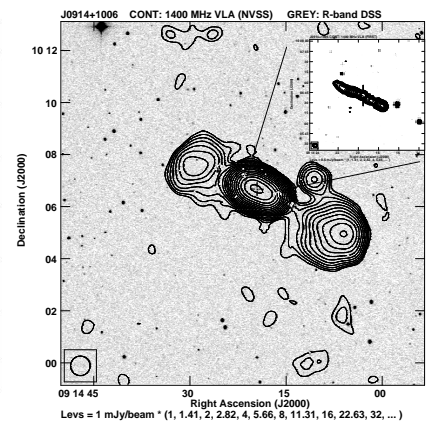
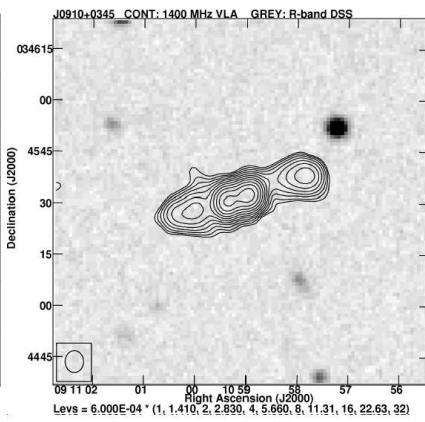
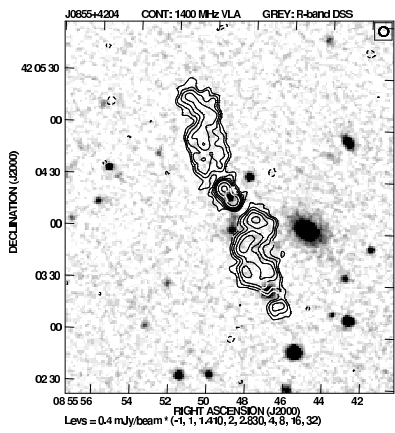
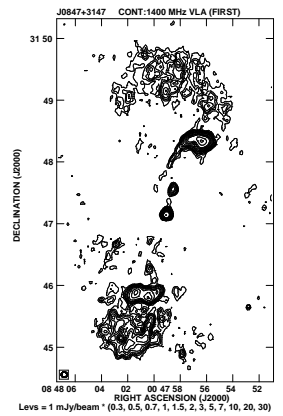
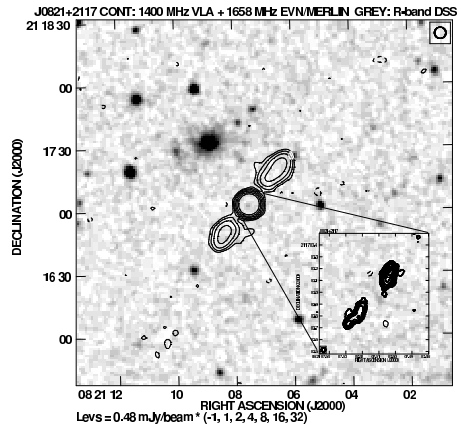
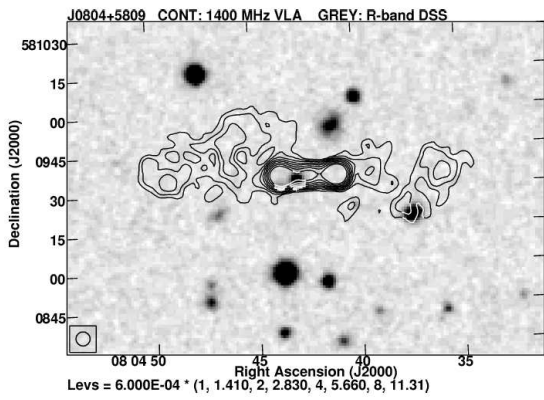
Notes: (a) a new DDRS; (b) flux density measured at 1.5 GHz; (c) This source is counted as radio relic associated with a giga-hertz peaked (GPS) source by Stanghellini et al. (2005) and by Shulevski et al. (2015). However, the optical DSS map (see the attached figure in the Appendix) reveals a weak extended emission in the vicinity of the extended diffuse relic. Therefore, in our opinion, the association is questionable. Deep optical observation are necessary; (d) triple-double radio galaxy; (e) the structure should be confirmed; the flux density of 1120 mJy is for the entire source; (f) X-shape radio source; (g) there are two nearby galaxies; identification consistent with FIRST is REC: 09^h29^m10^s.38 DEC: +41°46′44″.5 (J2000.0); (h) GHz Peaked Spectrum radio source; (i) Compact Steep Spectrum radio source; (j) Size of one side middle lobe; (*) – restarting radio galaxies with inner lobes more luminous than the outer ones.

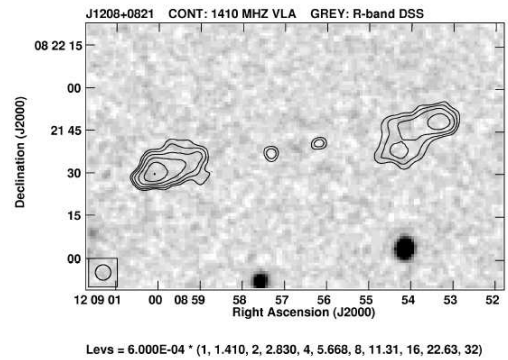
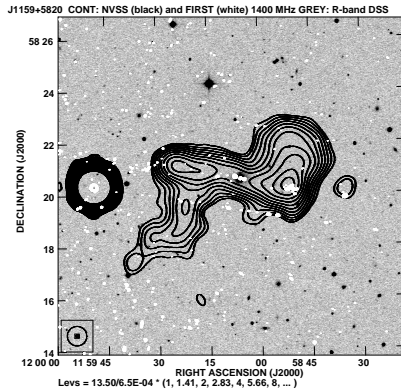
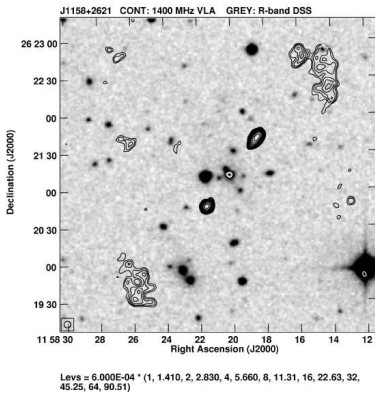
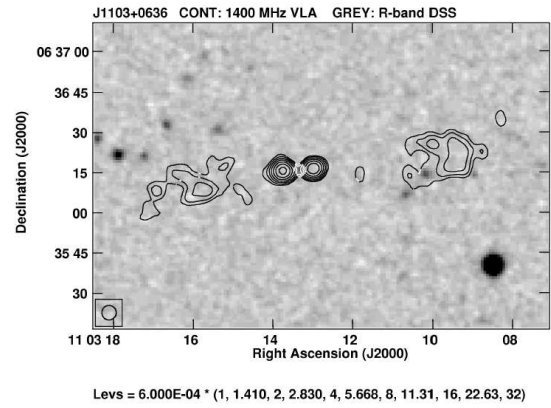
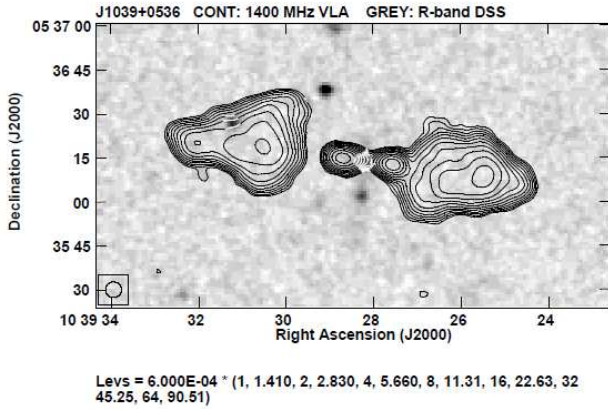
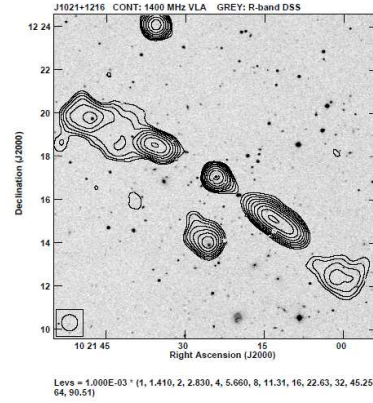
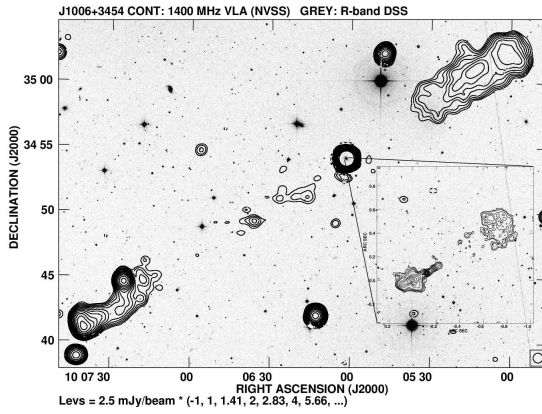
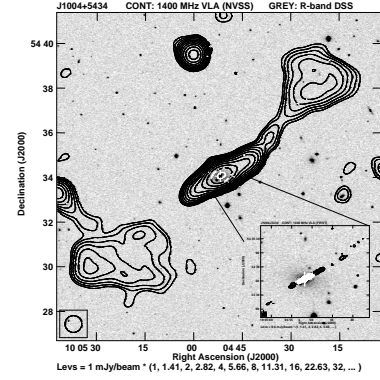
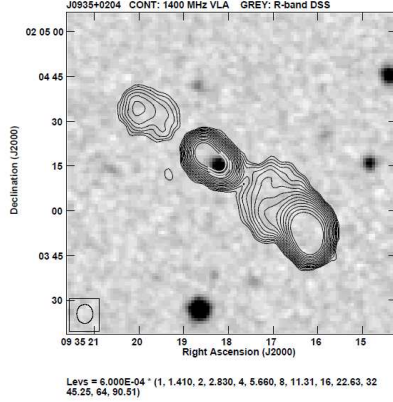
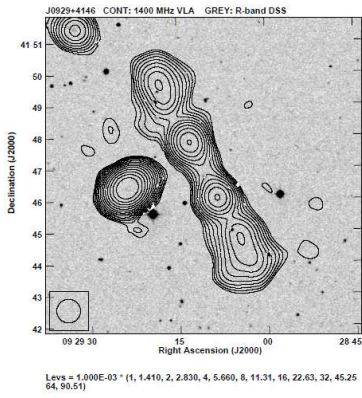
References: (1) Leahy & Perley (1991), (2) Shulevski et al. (2012), (3) Saikia et al. (2006), (4) Machalski et al. (2007), (5) Saripalli et al. (2012) (6) Baum et al. (1990), (7) Saripalli et al. (2002), (8) Shulevski et al. (2015), (9) Morganti et al. (1993), (10) Subrahmanyan et al. (1996), (11) Saripalli et al. (2013), (12) Siemiginowska et al. (2003), (13) Nandi & Saikia (2012), (14) Marecki & Szablewski (2009), (15) Jamrozy et al. (2007), (16) Giovannini et al. (2005), (17) Perley et al. (1980), (18) Bridle et al. (1986), (19) Clarke et al. (1992), (20) Machalski et al. (2006), (21) Brockopp et al. (2007), (22) Jamrozy et al. (2009), (23) Stanghellini et al. (2005), (24) Sikora et al. (2013), (25) Willis et al. (1974), (26) Strom & Willis (1980), (27) Schilizzi et al. (2001), (28) Owen & Ledlow (1997), (29) Koziel-Wierzbowska et al. (2012), (30) Schoenmakers et al. (2000), (31) Marecki et al. (2003), (32) Bondi et al. (2004), (33) Burns et al. (1983), (34) Clarke et al. (1992), (35) Bridle et al. (1981), (36) Hota et al. (2011), (37) Konar et al. (2006), (38) van Breugel & Fomalont (1984), (39) Saripalli & Subrahmanyan (2009), (40) Venturi et al. (2004), (41) Zhao et al. (1993), (42) Saripalli et al. (2003), (43) Safouris et al. (2008), (44) Ge & Owen (1994), (45) Colafrancesco et al. (2013), (46) Marecki et al. (2016), (47) Burns et al. (1982), (48) Roettiger et al. (1994), (49) Black et al. (1992), (50) Blundell & Fabian (2011), (51) Kronberg et al. (1986), (52) Leahy et al. (1997), (53) Bagchi et al. (2014).

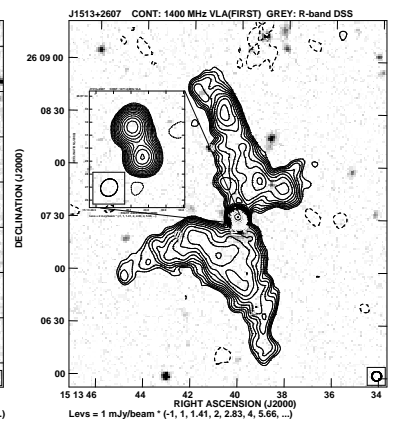
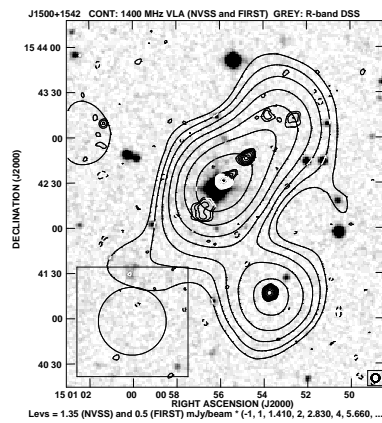
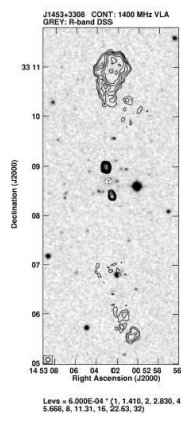
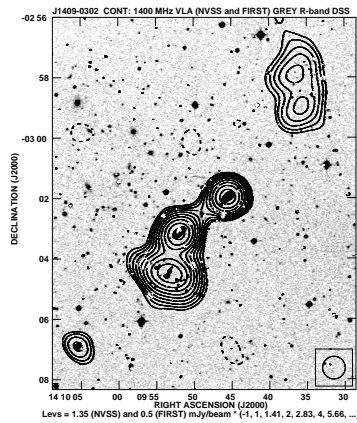
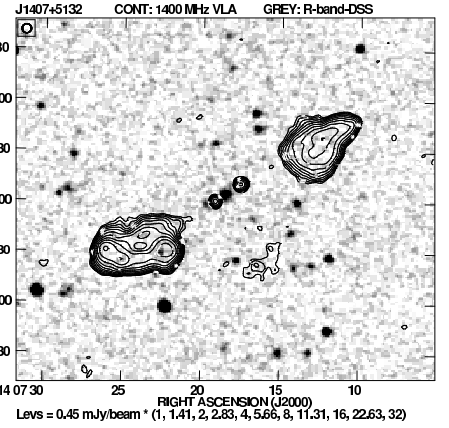
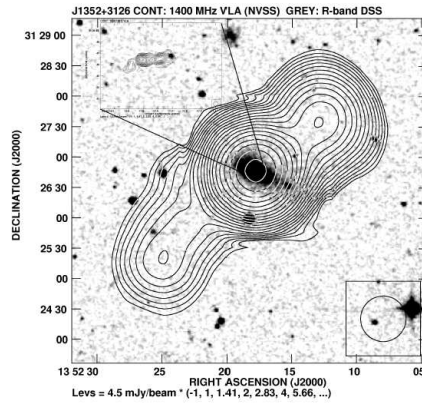
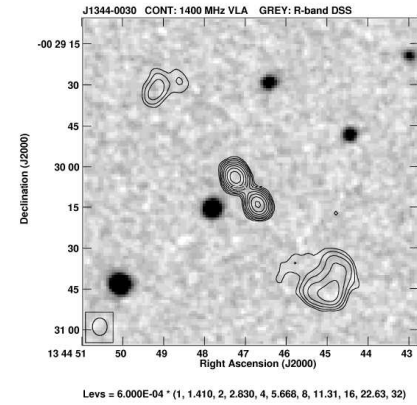
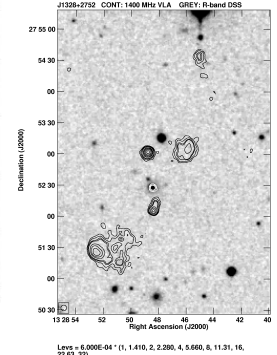
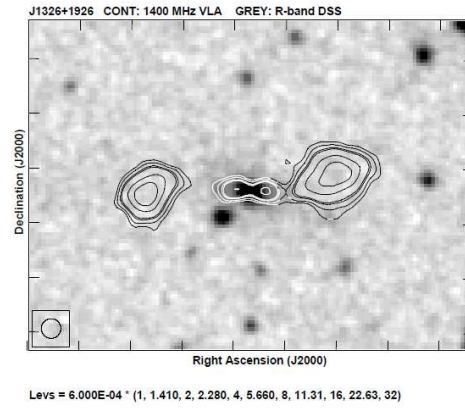
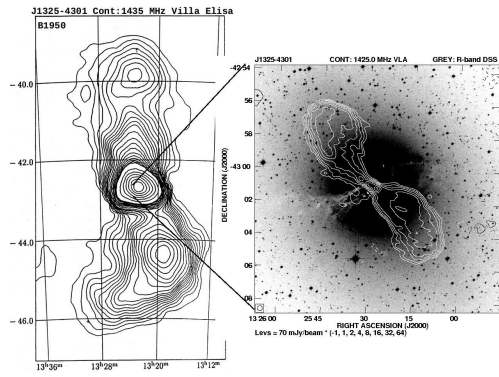
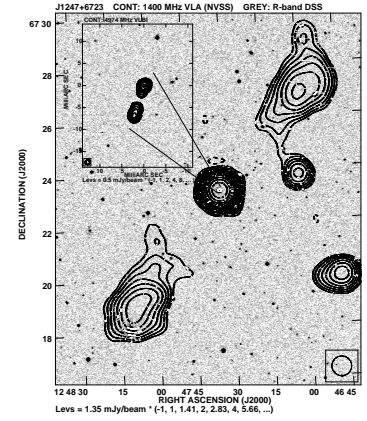
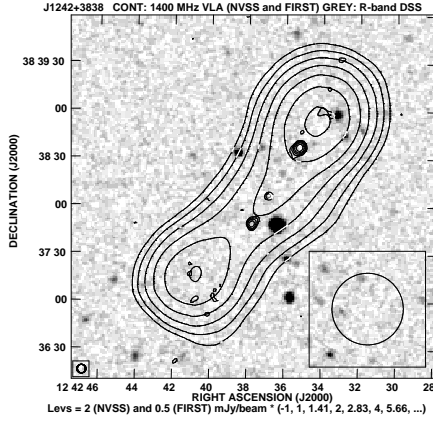
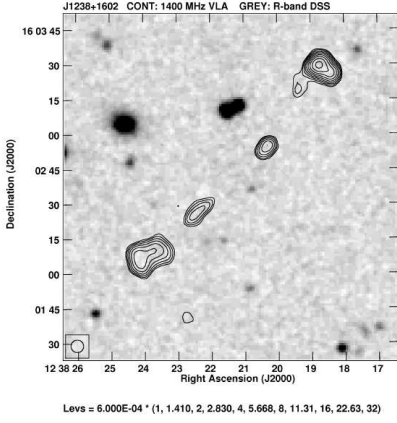
APPENDIX A: RADIO MAPS OF RESTARTING RADIO SOURCES – CLASS A

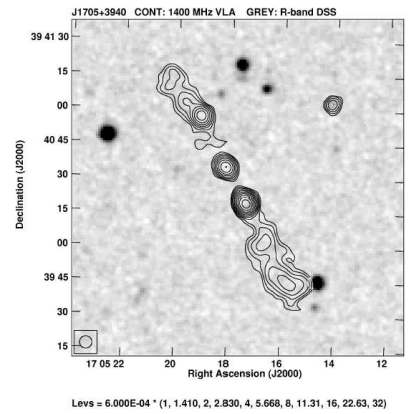
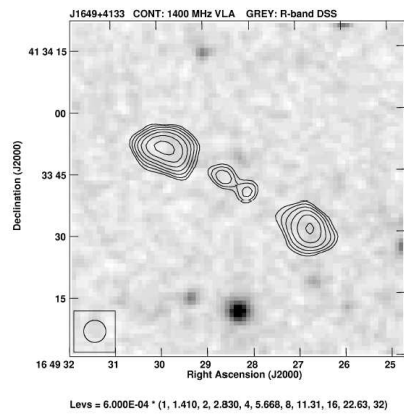
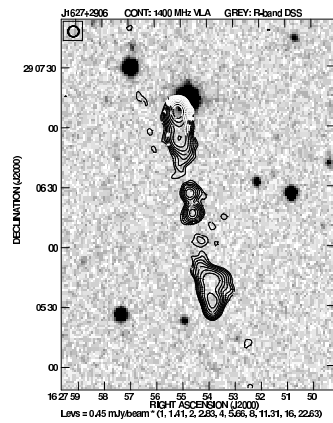
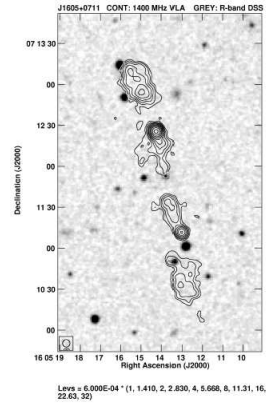
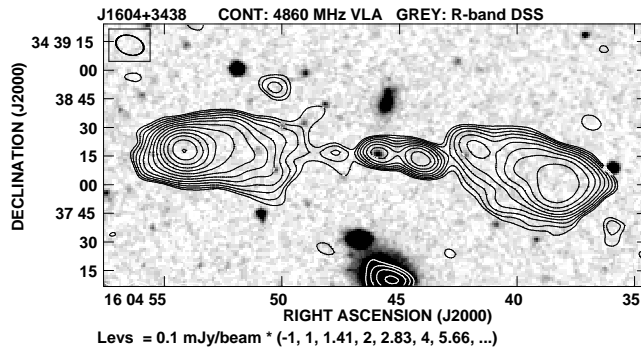
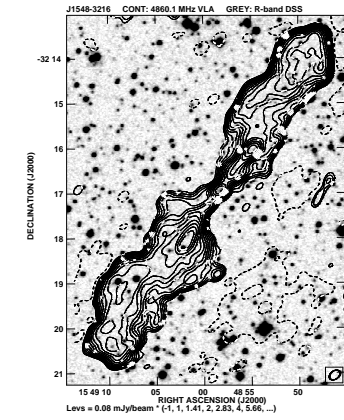
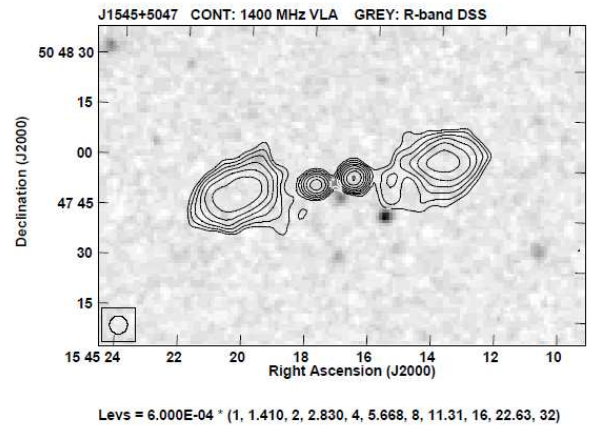
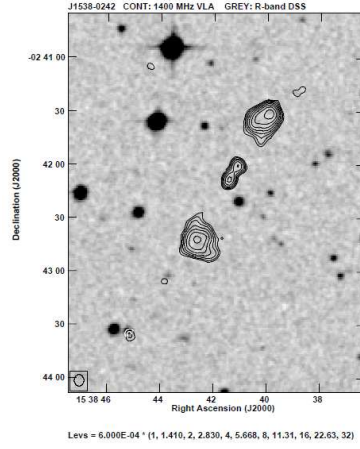
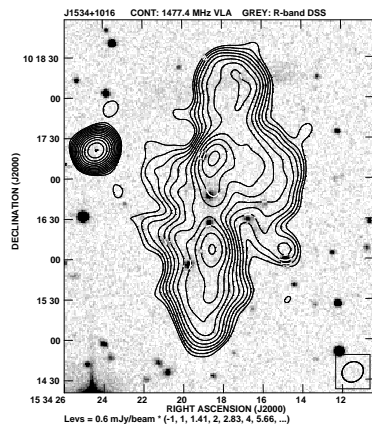
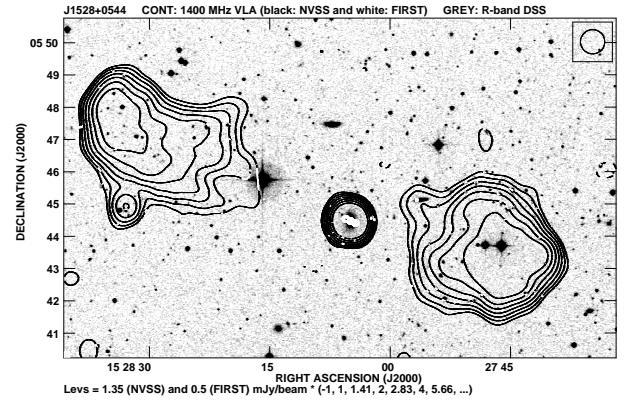
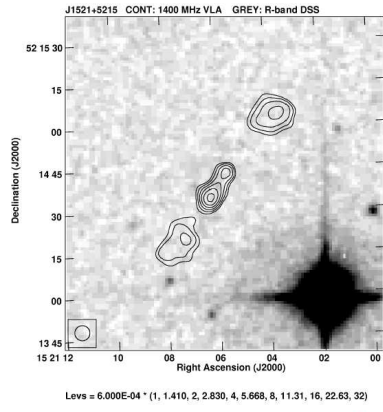
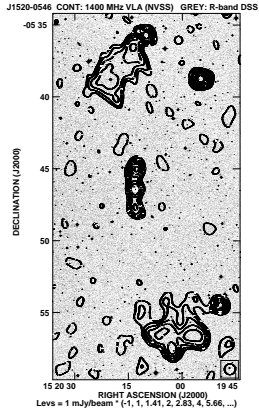
This appendix presents radio maps of restarting radio sources, which are of typical double-double radio morphology – class A sources. Most of the radio maps were obtained with the Very Large Array at 1.4 GHz. Maps of J0041+3224, J0351–2744, J0927+3510, J1648–3218, J1604+3438, J2107+2331 radio sources show radio contours at 4.8 GHz, and of J0037+1319, 2048+0701 at 8.4 GHz. The map of J0104–6609 was taken from (Saripalli et al. 2012). Three radio maps were plotted using data from other radio telescopes. The 330 MHz map of J0116–4722 was taken by Giant Metrewave Radio Telescope, the 1.4 GHz map of inner structure of J0821+2117 is from the EVN/MERLIN measurement, and the 4.9 GHz inner structure of J1247+6723 comes from VLBI. In all the cases the radio contours are overlaid onto the R-band optical image from Digital Sky Survey (DSS).

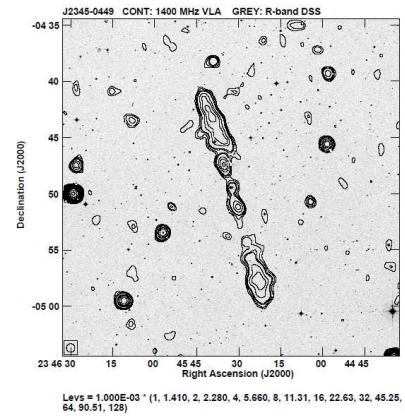
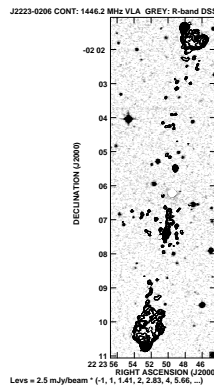
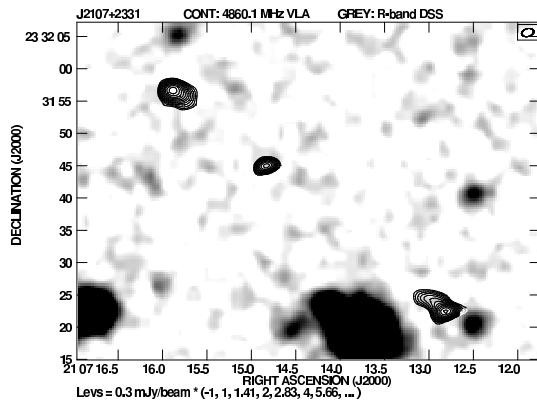
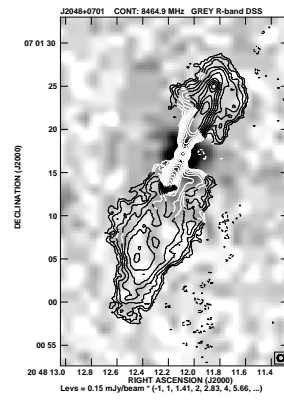
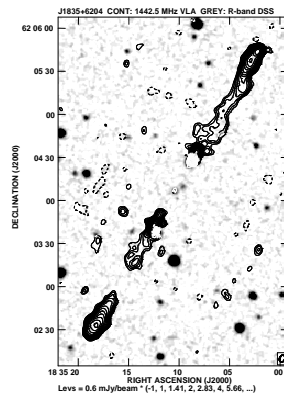
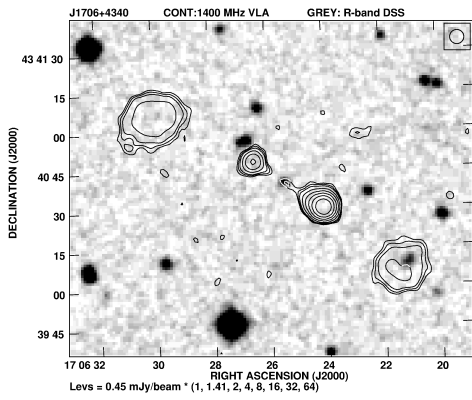












2 RADIO MAPS OF RESTARTING RADIO SOURCES – CLASS B

This appendix presents the radio maps of restarting radio sources with prominent inner structures surrounded by diffuse outer structures – class B. All of the radio maps presented here were obtained with the Very Large Array at 1.4 GHz. The map of J0301+3512 was taken from [Shulevski et al. \(2012\)](#). In all the maps radio contours are overlaid onto the R-band optical image from Digital Sky Survey (DSS).

This paper has been typeset from a $\text{\TeX}/\text{\LaTeX}$ file prepared by the author.

